10-29-2019

Advancements in Novel Material RFID-Based Crack Sensing and Bridge Weigh in Motion

Benjamin Bruciati
benjamin.bruciati@uconn.edu

Advancements in Novel Material RFID-Based Crack Sensing and Bridge Weigh in Motion

Benjamin Peter Bruciati

B.S., University of Connecticut, 2017

A Thesis

Submitted in Partial Fulfillment of the

Requirements for the Degree of

Master of Science

at the

University of Connecticut, 2019

APPROVAL PAGE

Master of Science Thesis

Advancements in Novel Material RFID-Based Crack Sensing and Bridge Weigh in Motion

Presented by

Benjamin Peter Bruciati, B.S.

Major Advisor

_____

Shinae Jang, Ph.D

Associate Advisor

_____

Kay Wille, Ph.D

Associate Advisor

_____

Richard Christenson, Ph.D

University of Connecticut

2019

ACKNOWLEDGEMENTS

First and foremost, I need to thank with all of my being my advisor, Professor Shinae Jang. You have provided all and more guidance needed by me to make this all possible. Without you, I would not have been able to complete this enormous task. You also have brought together an incredible group of people that form the UConn Smart Infrastructure Lab. This group of people have also contributed much of their time to aide me in research and writing. From the past members, Ned, Rosanna, Valeri, Leanna, Daniele, Sam, and Sean and from the current members, Pierre and Bartek. To both Pierre and Bartek, you both have supported me since you joined the team and I thank you for all your help and time.

Second, I would like to thank my advisory board of Professor Christenson and Professor Wille. I thank you for being a part of my defense. I have taken classes with both of you and I very much enjoyed them! Your expertise has shaped me into a better student and given me invaluable knowledge on my research.

I also wish to thank my fellow students not from the SIL. Dominic, Kevin, Sergio, Connor, Joe, Alex, Mike, and many others. At some point or another, all of you have helped me out in classes or research without a second thought. I hope for the best for all of you as you continue your education or in the workforce in the real world.

Moving on to the many professors that helped me on the way either in classes or just as a mentor. Professor Motaref, Professor Kim, Professor Malla, Professor Zaghi, Professor Burnicki, Professor Garrick, and Professor Zhang. Lastly, I must thank my family and friends that have stayed with me through it all. My time on Club Track helped me get down this long road and was a great experience. Also, my girlfriend I must thank. You have willingly dealt with me during this

whole time which couldn’t have been easy. My family has always been there for me which I can never repay, I wouldn’t be here without them.

TABLE OF CONTENTS

Page

LIST OF TABLES

Table Page

LIST OF FIGURES

Figure Page

ABSTRACT

The current infrastructure in the United States is continually deteriorating. Smart structures in civil engineering are becoming increasingly popular due to the performance enhancing systems they contain. Many of these systems are related to sensing and monitoring the structure. Structural health monitoring (SHM) has state of the art technological advances in both these fields. This thesis contributes to the advancements in the SHM field, particularly crack detection and Bridge Weigh-In-Motion (BWIM). The crack detection research uses existing radio frequency identification (RFID) crack detection technology and applies it to a novel material, Ultra High-Performance Concrete (UHPC). This system uses backscatter power to detect environmental change has been experimentally assessed in the lab for crack detection with varying crack widths of UHPC. BWIM is the use of an in-service bridge and its responses to detect vehicle characteristics of that vehicle traveling over that bridge. For BWIM advancements, speed calculation of trucks traveling over bridges is a main factor in many BWIM methodology. This thesis presents two speed calculation methods using one or two sensors to use in the speed calculation portion of vehicle weight determination algorithm. With this new algorithm, bridge response, and truck weight data, the vehicles weights are determined, and their performance are evaluated with two standardized specifications. These additions to the SHM community both present low cost and non-intrusive methods that gain insight into these smart structures to better maintain the United States infrastructure network.

CHAPTER 1. INTRODUCTION

The main goal of civil engineers is to design, build, and maintain infrastructure. The continued growth of our society is reliant on the transportation network and dependent on its integrity. This growth along with the aging infrastructure puts the integrity at risk. According to the 2017 Infrastructure Report Card (ASCE, 2017), the U.S. received a D+ for the overall infrastructure and a C+ for bridges. In fact, 9.1% of bridges are structurally deficient but are traveled over about 188 million times per day; And this number continues to increase. From 1970 to 2000 the number of miles traveled by combination trucks went from 35511 million to 134600 million, an almost 280% increase (U.S. Department of Transportation, 2016). These increasing traffic loads along with natural disaster impacts' these critical structures, and pose a major safety risk for the nation.

With the high costs associated with maintaining these crucial staples of the transportation network, bridge owners need to make the best use of their budgets. An estimated $18 billion was spent on bridge repairs in 2010 (ASCE, 2017) which is the highest spend of any year. Even with this increase in spending the current estimate for rehabilitation projects is estimated at $123 billion. With structural health monitoring (SHM), this estimate can be decreased. "Structural health monitoring is a multi-discipline field that involves the automatic sensing of structural loads and response by means of a number of sensors and instruments, followed by a diagnosis of the structural health based on the collected data" (Yuequan, et al., 2018). This tool can evaluate the health and safety of any engineered structure during normal and extreme excitation. SHM can re-evaluate structures in real time and identify what needs to be further investigated, lowering costs by performing meaningful repairs. Manual inspections, while primarily visual, are very expensive, time-consuming, and sometimes impossible depending on the nature of the

damage and the access, such as an abutment back wall behind a girder (Zhang, *et al.*, 2017). Many non-destructive techniques such as ultrasonic and eddy current pulsed thermography (ECPT) were developed to aide visual inspection, have acceptable resolution and reliability. However, these methods are costly and were not designed for large scale use. With the introduction of SHM these structures can be more accurately assessed and in a very time efficient manner. While SHM can accurately monitor the response of the structures, sometimes the loads can be difficult to ascertain.

Because of the intrinsic uncertainty of loads in the field, some SHM practices can struggle. One solution to this ambiguity is bridge weigh in motion (BWIM). BWIM is the process of using sensors on a bridge to measure the weight of the vehicles traveling over it, essentially using the bridge as a scale. Using the bridge responses that are collected from sensors, the weights, speeds, and counts of the vehicles can be collected. BWIM presents a more accurate number of the actual loads and number of times these loads occur, cyclic loading as it will be referred to. In Connecticut, currently the traffic count data is commonly referred to as ADT (Average daily traffic) and comes from the state traffic log. For structure specific locations, such as bridges, this is used to estimate the number of cyclic loading the bridge will experience. This practice however, is inaccurate because the ADT is only an estimate and in the traffic log it states "The ADTs shown should not be used for point-specific locations" (Division of Systems Information, Bureau of Policy and Planning, 2015). Introducing a reliable BWIM system on a bridge will give very accurate truck counts and cyclic loads from the trucks on that specific bridge. Truck counts are more important than total vehicle counts due to the higher impact trucks have on a bridge when compared to lighter vehicles. Using this newly obtained, bridge specific data, the bridge owners can design more efficiently, assess damage, and repair more cost

effectively. However, some SHM methods aren't dependent on knowing the amount loading on the bridge.

More local SHM methods don't rely on knowing the global characteristics of the structure to accurately assess. Crack detection is an example of this local SHM strategy. The detection of cracks in a structure is essential to the long-term health of said structure. The previously mentioned cyclic loading that a bridge structure experiences creates one of the most common cracks, a fatigue crack. Despite the fact that engineering components and structures are carefully designed against fatigue failures, more than 50% of mechanical failures are due to the formation of fatigue cracks (Zhang, *et al.*, 2017). Common crack detecting techniques use long lead cable arrangements for data collection which can be cumbersome and tedious to maintain (Kalansuriya et al., 2013). Low cost wireless sensors became the most attractive solution to solve the restrictions of the previous methods. Originally designed for large scale asset tracking (Zhang, *et al.*, 2017) radio frequency identification (RFID) technology can fill this new role in SHM due to its unique capabilities. Ultra-high frequency (UHF) passive RFID tags are wireless, low cost, and easily deployable in high numbers. These tags have the capability to track the permanent change in impedance and radiation caused by a crack. Therefore, when a material under and around the tag changes, the loss of that material can be monitored. This capability makes RFID a viable crack sensor. While this sensor has been tested on concrete and steel, both of which are common and time-tested construction materials, a more novel material has yet to be monitored.

Ultra-high-performance concrete (UHPC) is a relatively new division of metal reinforced concrete that, in its present form, became commercially available in the United States in about the year 2000 (Graybeal, 2011). The Federal Highway Administration (FHWA) began

investigating the use of UHPC for highway infrastructure in 2001 and has been working with the transportation departments of the states to deploy the technology since 2002 (Russell and Graybeal, 2013). Currently, the most popular application for UHPC in prefabricated bridge construction in the U.S. is in the connections between prefabricated bridge deck elements. With the increasing popularity of using UHPC for building columns, bridge girders, for structural repair, etc., more uses for it are being found (Ataur and McQuacker, 2016). Its material properties make it a more feasible material for bridge connection joints and structural repair. The introduction and increasing use of this new material has come with new maintenance and structural health monitoring (SHM) practices. Using SHM, these new applications for UHPC can be evaluated.

In this thesis, two systems to further the progress of SHM will be presented. In chapter 2 a comprehensive literature review of SHM, UHPC, RFID, and BWIM will be presented. Chapter 3 contains RFID based crack detection research involving UHPC as the cracked specimen. Chapter 4 describes research on a BWIM algorithm on a bridge in Meriden CT. The system was implemented onto the bridge in previous research. Chapter 5 contains the conclusions that came from this research. Chapter 6 outlines suggestions and actual future work to be done to further this research.

CHAPTER 2. LITERATURE REVIEW

This chapter provides a thorough literature review on the topics of BWIM and RFID crack detection. This includes the history of BWIM, current and previous European studies, and more recent BWIM projects, Connecticut's research being some of them. RFID technologies origin's and the current research related to crack detection is reviewed as well.

2.1 Structural Health Monitoring

As civil engineers, the amount of risk of failure involved with civil structures is low comparably to something such as a manufacturing machine (Aftab and Karim, 2018). With this low risk levels, where does it come from? As a society, these structures are not expected to fail even during high intensity situations such as hurricanes or earthquakes. Each of these structures are unique as opposed to a mass-produced item and as such, don't have the time-tested data of a manufactured prototype. Due to that nature, the service life and structural interactions are difficult to forecast. SHM can eliminate these unknowns and with that, can decrease the actual risk of failure for these structures. With this reduced risk also comes with a reduced cost to society; this due to the capital to construct and maintain its society. Currently structures that are inspected regularly, such as bridges, to determine their integrity create high time and monetary costs for the structure owners. These methods can often be visual, which due to human error, can be inconsistent. With increasing pressures to minimize maintenance cost and reducing in-service failures, smarter SHM techniques have been developed.

"Structural health monitoring is a multi-discipline field that involves the automatic sensing of structural loads and response by means of a number of sensors and instruments, followed by a diagnosis of the structural health based on the collected data" (Yuequan, et al., 2018). To be able to perform all these, there is 4 branches of SHM methods. Detection of the existence of damage, localization of the damage, quantification of the damage severity, and determining the remaining life of the damaged structure (Carden and Fanning, 2004). Together, these can create a real-time idea of how the structure is performing. Traditionally, most of these methods involve placing sensors such as accelerometers, strain gauges, piezoelectric sensors, ultrasonic wave sensors, and many more (Sony, Shea, and Ayan, 2019). The sensors capture the behavior of the structure than can mostly be unseen by the human eye. These sensors and most SHM techniques fall into the Non-Destructive Evaluation (NDE) identification. While these contact-based sensors have the advantage of generally being cheaper and more, straight forward to use, there are advantages of wireless sensors.

Wireless sensors fall under the NDE section as well. These sensors avoid the connection via server cable, which can be costly and can hinder data collection based on the surrounding conditions (Straser and Kiremidjian, 1998). In buildings, some members may become inaccessible once the building construction is completed. Cases such as these can employ wireless sensors like RFID for condition assessment. Along with breakage-triggered strain sensors to detect the strain. These two technologies utilize the wireless sensing technologies where information can be recorded from a distance. Another system that used wireless sensors was Huynh *et al* (Huynh, Kim, and Lee, 2016). They used wireless sensors which then implemented stochastic subspace identification (SSI) analysis and time-frequency short time Fourier transform (STFT) method to analyze and update the structural parameters. The modal

parameters were found out after mounting the accelerometers on a bridge. It was discovered that with an increase in wind speed, the natural frequencies reduced due to loosening of cables and increment of flexibility (Swagato and Purnachandra, 2018). Typical wired accelerometers can measure three-way acceleration and are economical and easily installed. A drawback, however is that these sensors are known to consume much energy and have limited resolution range (Kilie and Unluturk, 2015). For the research performed by Kilie and Unluturk, they used rechargeable wireless accelerometers. All sensor readings matched each other, validating the short-term vibration effects on a wind turbine. Of course, a con to this system was that interference from electromagnetic radiation could affect the accuracy. In this situation, wired sensors may not be appropriate, but this would reduce the effect of interference.

As mentioned before, wired sensors can have their benefits as well as their wireless sensor counterpart. A popular sensor type, the fiber optic sensor, has become more mainstream in past years. Chen *et al.* have used one of these sensors to great success (Chen, Wu, and Feng, 2019). This sensor can be applied to the structure, when connected to its interrogator, and have multiple uses. The typical use for a Fiber Bragg Grating (FBG) sensor is to capture the strain response in a large region of the structure. Because of the "Wired" nature of this sensor, it can be laid out all down a girder and tell the strain of multiple places on the girder with only the one sensor. Another reason wired can fit the system is the average cost. While these sensors have been on the market much longer than wireless so they have had time to decay in price. Particularly electrical strain sensors are inexpensive and are also suitable for dynamic loads (Swagato and Purnachandra, 2018). If an internal strain sensor needs to be used, such as embedded in concrete, there is also a cement-based strain sensor. Used mostly for UHPC, this

sensor is a high strength smart sensor that bonds naturally with the parent structure (Azhari and Banthia, 2012).

One branch of SHM is related to detecting the existence of damage. While this seems intuitive, hard to access areas or damage that is unseen by the human eye can are both valid instances to use SHM methods. Both the wired and wireless sensor sets can perform this as well as other SHM techniques like vision-based that can involve machine learning (Swagato and Purnachandra, 2018). A principle parameter to detect damage is to detect a change in strain. This may be cause by change in temperature, compression forces, cyclic loads, and others. A few sensor types to measure strain were mentioned before, but one type of sensor doesn't use this principle to detect damage or cracks, RFID.

2.2 RFID based crack detection

The United States infrastructure has been slowly decaying and with more than 200,000 of them being more than 50 years old (ASCE, 2017) that is to be expected. The current estimate of 123 billion dollars to fix the bridges is a high price. As stated by the Federal Highway Administration (FHWA), all bridges must be inspected every two years. The program was developed in 1968 by the Federal-Aid Highway Act (FHWA, 2004). This method, however very straight forward, can sometimes be ineffective and unreliable depending on the inspectors' experience. While there is also NDE methods such as eddy current, radioscopy, and lamb waves that are based on scientific principle, these can be costly and need much labor to be installed and maintained. (Sun, Li, and Ye, 2010). With these in mind there leaves much more to be desired.

Concrete accounts for more than 60% of the current bridges built annually in the USA (Aktan, *et al.*, 1999). Cracking is very prevalent in concrete bridge structures. Out of the over

600,000 bridges in the USA currently about 410,000 of them are made of either concrete or prestressed concrete. (FHWA, 2017). With these two bridge types being the most common, large amounts of concrete, reinforced concrete (RC), and UHPC are needed. Cracks in members can be classified into two main categories, (Leonhardt, 1977) cracks caused by externally applied loads and cracks that occur independent of loading conditions. Both types occur in various locations all over the bridge ranging from the deck to the abutments. Just one of the locations that cracks are located is on a box beam bridge. In 2008 a survey of state agencies said that 76% of box beam bridges had the most common crack at the interface of the grout and box beam (Russell H. , 2009). While visual inspection can catch these cracks if they are large enough inspection can sometimes be dangerous or the location can be difficult to access. Locations such as behind girder ends and cracks on the bridge deck with moving traffic.

Recently, NDE techniques have generated great interest in the field of SHM as they do not affect the structural integrity of the bridge. Microwave techniques can retrieve information by reflected electromagnetic waves. These techniques can require much computational time and resources and therefore are not suited for real time monitoring (Donelli, 2018). A cheaper method would be RFID-based tag crack sensors. RFID is a well-known technology for asset tracking and unique ID attachment and can be useful in SHM applications. RFID is a system which is based on a tag which demodulates a low frequency interrogating signal provided by the reader. In particular an RFID tag transmits data to the reader introducing a modulation on the back scattered wave by means of a proper variation of the load impedance of the antenna tag. RFID tags are quite cheap and require no maintenance, prices ranging from $0.02-$0.06 and still decreasing. This easily deployable system has already seen use in various positions on various materials.

Previous research of crack sensors by Kalansuriya (Kalansuriya, Bhattacharyya, and Sarma, 2013) and Martinez-Castro (Martínez-Castro, Jang, Nicholas, and Bansal, 2017), while successful on both concrete and metallic materials, respectively, lacks the validation of testing with UHPC. This system used passive RFID technology but with key modifications, such as the removal of the substrate material and the use of a volume-based index rather than just crack width and length like many other inspection procedures. So far, a system with low cost, field ready applicability and testing does not exist. The ease of large-scale deployment, the low cost and the inspection feasibility of the 1 ft. (30.48 cm) read distance make this an ideal tool for transportation agencies to monitor these new UHPC retrofits. Other previous research, by Zhang *et al*., outlines a system that can assess the condition of a structure through the use of RFID tags. This system, while having been successfully tested on PVC tubes, also lacks testing on UHPC. The system also requires a more complex strain sensor setup and unique conditions such as conductive paint and the placement of a material referred to as a brittle bar (Zhang and Bai, 2015). The ease of placing a sticker-like tag that could be seen by a technician and the ability to place it anywhere on UHPC section without any major surface changes, like painting, could increase the range of locations where this system could be implemented. This section shows the applicability of RFID tags as crack sensors for UHPC. The cracks were located on UHPC specimen sections. The crack was simulated by saw cut and increased in volume at each damage stage. The damage sensitivity was determined by the ability of the tag to return different backscatter powers as the crack volume in the UHPC specimen changed. The backscatter power was then measured by two different methods in lab scale experiments. The system was able to perform the crack monitoring even with adverse effects from the UHPC. The total damage index showed the change in backscatter power and was used to quantify the results.

Passive Ultra High Frequency (UHF) RFIS sensors have been a popular sensor type due to their ease of use, low cost, and low maintenance. The flexibility of the tags is another positive of these sensors. One research showing the benefits of a passive system is with a RFID sensor was placed on a flexible foil for ball pressure monitoring. The sensor was placed on two different sports balls and with the passive nature of the tag, the ball could be used as normal without any wires. The tag could also withstand any forces the ball undergoes during normal use. The ball pressure was able to be determined after reading it and the ball holder wouldn't have even known the sensors presence. (Rennane, *et al.* 2018). More reaserch that uses a passive system was published in 2012. This research uses a chipless design to montior crack detection. The chipless has the advantage of having an even lower cost than chip tags and are fesible for large surfaces like bridges or roadways. Using the backscatter power method, the chipless tag concept is considered fesible when used to detetc the length and oritentation of the crack (Kalansuriya, *et al.*, 2012).

Several studies have been performed on the development of RFID crack sensing technology. One project works with a conductive surface RFID sensor with a substrate. A substrate can be common as it will transfer the strains to the tag without affecting the strain if possible. When cracking occurs, the substrate is strained which in turn, strains the tag. What makes this sensor different is that when cracking occurs the electrical resistance of the conductive surface increases and in response, the RFID sensor (Pour-Ghaz, et al., 2014). The study showed that with the addition of the conductive surface, the crack width can also be monitored. A calibration of different crack geometries would be needed. Another research piece was by Martinez-Castro, who also used the substrate in their method. This research focused on metallic materials, while the last one mentioned focused on concrete. The substrates use, like the

last study was to transfer the strain to the tag, but also to maximize the power received by the antenna. This was done because the reflected wave can be maximized when the reflection of the RFID tag comes from half a wavelength away. (Martínez-Castro, Jang, Nicholas, and Bansal, 2017). The sensor was successful in its lab scale performance while using the percentage change from the undamaged stage as a damage index.

These show the promise and flexibility of RFID systems and that it can be made to apply to many situations. The use, or not, of a substrate, the passive power harvesting nature, the tag flexibility, and low cost are just some of the benefits mentioned here. With this wide range of uses, no such sensor has been applied to UHPC. Use on UHPC will add many different variables into the system and needs to be tested.

2.3 Ultra High-Performance Concretes (UHPC)

Concrete is one of the most widely used building materials worldwide (Acheampong, *et al.*, 2013). The first use of iron-reinforced concrete was by the French builder François Coignet in Paris in the 1850s (Chang and Alfred, 2017); ever since then, reinforced concrete has been a staple of modern construction. However, because of its poor tensile resistance and cracking behavior, researchers hare intent on developing a new cementitious material that could replace or strengthen the reinforced concrete for infrastructure.

The maintenance of aging infrastructure is critical to achieve the designed structure life. Corrosion damage affects 15% of the nation's bridges (ASCE, 2017) and is severely shortening their service life. This damage is particularly severe at the girder ends. This is where water and

deicing materials leak through the joints and create section loss at the ends. This section loss reduces the thickness of the web plate near the supports and affects the baring capacity of these girders (Jin-Hee, Shigenobu, and In-Tae, 2013,). The current repair procedure is time consuming and costly. New methods, proposed by Kennedy and others, look to use UHPC as a retrofitting. With Kennedy's UHPC jackets having only been implemented in June 2014 (Doiron, 2016), this new repair method needs to be studied in the field long term. With much focus on numerical simulation, for the future use of UHPC, by researchers like Huang (Huanghuang, Xiaojian, and Ailian, 2018) and Liu (Liu, et al., 2018), the already in-place structures lack the required attention. Current retrofits like Kennedy's increase the section size, which can cause unknown forces or transfer previous ones. These retrofits are missing the SHM technology required for maximizing maintenance procedures in terms of time and these new forces. A traditional monitoring method would be via electrical resistance strain gages. This method, while accurate, is costlier and more prone to damage during and after installation (Song, Li, Wang, and Ho, 2017).

Ultra-high-performance concretes (UHPC) are utilized for applications such as bridges, pavement overlays, and tall building columns (Russell and Graybeal, 2013). These applications sometimes call for UHPC over normal reinforced concrete (RC) due to its material properties. UHPCs are cementitious composites characterized by high compressive strength, low water binder ratio, and optimized gradation curves (Graybeal, 2011). In many cases, thermal activation, fiber reinforcement, and superplasticizers are employed to increase strength, enhance ductility, and ensure workability (Wan-Wendner, Wan-Wendner, and Cusatis, 2018). Specific characteristics that distinguish UHPC from RC include compressive strength above 21.7 ksi (150 MPa) and pre-and post-cracking tensile strength above 0.72 ksi (5 MPa). Fatigue tests of UHPC

specimens under various combinations of stress level and stress range showed a range from 2.5 to more than 7.0 million cycles (Russell and Graybeal, 2013). At the lowest end of this range, this fatigue life was about 80% more than RC (Ekenel, Rizzo, Myers, and Nanni, 2005). The fibers contained within the concrete had a large impact on the tensile capacity. The steel fibers improved the flexural moment capacity, stiffness, and cracking behavior of the UHPC beams, but the crack localization caused a reduction in ductility. This phenomenon can occur in both normal and high-strength concretes containing steel fibers and conventional reinforcement (Hasgul, Turker, Birol, and Yavas, 2018). These characteristics show the advantages of UHPC over RC, but at a cost.

UHPCs have a higher monetary cost than RC due to the difference in material properties. The commercially available product is a proprietary blend sold for about $2000/yd3 ($2600/m3) versus the conventional concrete which is about $100/yd3 ($130/m3) (B., 2013). Given that UHPC is 20 times more expensive than conventional concrete, it is generally used for retrofitting rather than massive construction. Although it has a higher performance, UHPC has minor drawbacks such as early-age cracking during the manufacturing process, due to the high cement content and highly exothermal hydration reaction (Shim, 2005), and cracking, caused by secondary forces such as temperature and shrinkage loads, during and after the manufacturing process (Haber and Graybeal, 2016). During a retrofit, a structure can experience unusual forces and, after the retrofit is complete, this new added section can experience unknown forces from section size change or structure material UHPC interactions. These unknown variables cannot always be accounted for; therefore, unintentional cracking can occur during and after retrofitting. Cracking can lead to exposure of the fibers to the elements. This greatly decreases the tensile capacity of the UHPC. Once exposed, cracking would make the retrofitting unreliable if the

beam was still exposed to the environment. Luckily, if the metal content and length are increased, shrinkage crack surfaces are considerably reduced, up to 86% compared to non-fiber specimens (Saradar, *et al.* 2018). With timely crack detection, these cracks can be identified and repaired before significant damage to the inner fibers occurs. Because the location of UHPC-retrofitted spots would be known, the detection of cracks with the low-cost RFID is feasible. This would improve UHPC's reliability.

2.4 Bridge weigh in motion

The first mention of Bridge Weight-in-Motion (BWIM) was by Moses in 1976 (Goble, Moses, and Pavia, 1976). The idea of BWIM was postulated for its large number of truck weight performed economically and the avoidance of avoid weigh stations. Three years later, another study was conducted. During this study, the feasibility of "weight-in-motion concepts using instrumented girders" was concluded as a valid method (Moses, 1979). Since then, numerous studies have been conducted and with them, a variety of methods to try to obtain these truck weights have been created. With these new methods, a way of classifying how accurate they are needed to be introduced. Europe, can seem further ahead than the rest of the world with many methods and studies created there. One of the most important programs that has come out of Europe's innovation is the Cost 323 and Wave programs.

In the 1990's there was no official specifications for WIM standards in Europe. Moreover, the US standard on WIM (ASTM, 1994), was mainly designed for model approval or to indication the max potential of a system when road conditions are optimal (COST 323, 2002). The goal of the COST 323 management committee's report was to cover the need of a complete

specification. This would include the modal approval, on-site acceptance test, and accuracy measurement that neither ASTM nor previous European standards contained comprehensively. The complete specification included a glossary, accuracy grading system, vehicle classification system, along with various other chapters. The accuracy grading system was divided into seven classes. Class A, B+, B, C, D+, D, E which correspond to a GVW percent accuracy of ±5, ±7, ±10, ±15, ±20, ±25, and +30 for a 95% confidence interval, respectively. The grading scale of the WIM systems was developed in respect with the application, like vehicle counting and fatigue assessments. Only class A and B+ are able to be used if legal purposes, such as overweight vehicle enforcement, is involved (COST 323, 2002). The report also developed criteria for optimal BWIM sites. The optimal span length of 5-15 meters (16.4-49.2 feet), with an acceptable span of 8-35 meters (26.2-114.9 feet). The skew should be less than 10 degrees with an acceptable range up to 25 degrees. The pavement before and on the bridge should be even and the bridge should be free of traffic congestion. During this project, it was realized that more research was needed to accommodate the latest WIM technology and needs of the road managers.

The Weighting-in-motion of Axles and Vehicles for Europe (WAVE) project began in 1996 and emerged from the need for further research on WIM during the COST 323 program. During 33 months, a group of 15 senior scientist and 25 Ph-D, students, post-doctoral, or young researchers and engineering's, along with many technicians worked on the Wave project (WAVE, 2001). The outlined three main goals of WAVE were accurate estimation of static weights using WIM systems, Quality, management, and exchange of WIM data, and the consistency of accuracy and durability. Within these were 9 subcategories and the result were

two seminars, another presentation at the Second European Conference on WIM, and an openly available website report that is now merged with the COST 323 website (WAVE, 2001).

As mentioned before, a large number of research studies have been devoted to BWIM technology. Connecticut specific projects will be mentioned in the next section. Every BWIM system is different and is trying to account for specific variables. Due to the complexity of BWIM, not all variables can, right now, feasibly be all accounted for. The first systems to be mentioned are the non-conventional, or non-contact sensor, BWIM systems.

Contactless BWIM is one of these systems. Using a high-speed camera, with an attached telescope, the deflection is captured and then motion tracked using a digital correlation method (Ojio, *et al.*, 2016). In theory, this creates one of the traditional methods, strain time history, but just in a different fashion. The research was able to capture the GVW relatively if the calibration truck was used recently. A restriction of this system is the camera. The vehicle needs to be moving slow enough for the camera to capture enough frames to be counted to calculate the speed. As well as an ample light source needs to be near the camera, so night monitoring is not very applicable. Another system proposed by researchers from the University of Minnesota look to use Microwave radar (Kumar, Schultz, and Hourdos, 2018) sensors. Also looking to track displacement, this is in theory and no actual research has been performed. The high accuracy and lower cost are acknowledged as potential. The researchers also acknowledged the use of infrasound as a potential sensor. A researcher in Connecticut used this and it will be discussed later.

Using accelerometers is another method for BWIM. One of the research projects done is on a bridge in Tokyo. The bridge consists of 2 lanes and 3 girders. Using accelerometers placed at different parts of the girder, like the vertical stiffener and main girder edges, the displacement

of the truck is obtained (Sekiya, Kubota, and Miki, 2017). From there, the speed and axle weights were obtained to get the influence line. The portable system of only accelerometers was able to determine GVW by 15% above or below. Unfortunately, like many systems the multiple presence variable was not able to be controlled. Also, the test trucks were the only vehicles tested, along with using speeds only below 30 MPH. Another accelerometer-based system is on a 590.5 foot (180 meter) long bridge in Korea. Using 20 accelerometers at a possible 50 different locations, the modal analysis was attempted (Kim, et al., 2009). Using frequency domain decomposition, mode shapes were successfully obtained from three different sensor topologies. An interesting discovery was that depending on the road roughness and velocities, the researchers looked at the body-bounce and wheel-hop vibration of the trucks. These occurrences are known to happen, but not much research has looked into it.

Strain time history is a very popular method for BWIM. Two research papers will be looked at. The first was tested on a bridge in Alabama in 2014. This nothing on road (NOR) system has strain transducers mounted on the bridge slab to detect the vehicles. Two different locations for sensor placement were used. The first was the weighing sensor which were mounted on the soffits of each girder along a line in the direction of the bridge to determine axle loads and GVWs. The second was for the axle detector and that was installed under the slab to obtain information on axle spacing and speed (Zhao, *et al.* 2014). When the influence line was estimated, the estimated GVW were also estimated to reasonable values. One restriction of this research is the very low sample size of 10 on lane 1 and 9 on lane 2.

The state of Connecticut has done much work in the field of BWIM. The most recent was mentioned before and is the use of Infrasound for SHM. When traffic crosses a bridge, it creates vibrations and that is making acoustic signals though the air. Using a microphone to measure the

sound pressure, the pressure is then transformed into voltage. With that, the dynamic bridge properties can be extracted from the PSD functions as a substitute for mounted sensors (Lobo-Aguilar, 2018). The same researcher performed analysis on 3 other bridges all with BWIM intent. Using strain, acceleration sensors, and strain rosettes GVW and speeds were determined with reasonable accuracy. The research demonstrated the BWIM applicability of a broad range of bridge types in CT. The last research in this review is a basis for the research presented in this paper. Wall used the method proposed by Ojio and Yamada (Ojio and Yamada, 2002) which uses strain sensors directly located on the steel girders beneath the bridge. This method requires no need for an influence line be calculates all needed information from the strain response data (Wall, *et al.* 2009). Using a calibrated beta value that comes from using a calibration truck, the speed, beta, and strain plot area are the 3 things needed to obtain the GVW. This study showed that the non-intrusive BWIM methodology shows promise. The beta value, however is bias on the type of vehicle used to create, or calibrate, the value. With this already in mind, the method can be improved, which is one of the goals of this research.

CHAPTER 3. RFID-BASED CRACK DETECTION OF ULTRA HIGH-PERFORMANCE CONCRETE.

3.1 Introduction

This chapter will provide the information about the research study using a RFID based crack sensing tag on a sample of UHPC. Background information about RFID technology, backscatter power, and damage descriptions will be included. The specimen and damage induced on the sample will then be described. From here, the actual testing and measurements will be introduced and explained with the conclusions to the study following.

3.2 Theoretical Background

The theoretical background behind the crack sensor is summarized in this section. The use of backscatter power for this passive RFID tag was based on the wave equation. The RSSI, could then be obtained and used later, as a measured value, for crack detection. The RSSI was then compared to a new damage index that related to the volume of the crack. Using the shape of a right triangular prism, the crack was idealized and able to be quantified into a new volume-based damage index. With the new damage index and RSSI, comparison of the two was done with the total damage index. This related the RSSI of the undamaged and the damaged state. The form of the total damage index could bypass the variability issue of the RFID tags by using only its own RSSI values as the comparison. This damage index can then be related to the volume index for a means of crack quantification.

3.2.1 Backscatter Power

The antenna-based crack sensor is based on the idea that when a crack appears, it permanently changes the radiation and impedance characteristics of the antenna (Kalansuriya, Bhattacharyya, and Sarma, 2013). In this research, the ultra-high frequency (UHF) passive RFID tag crack sensor uses this idea and treats the backscatter power as the crack measurement unit. Passive refers to the tag either harvesting or receiving power from a power read-out unit during data collection (Caizzone and DiGiampaolo, 2015). Backscatter power is identified as the most important measured value for crack detection (Kalansuriya, Bhattacharyya, and Sarma, 2013). This power comes from the transmitted power of the antenna which is then transferred to the tag. The tag then sends the power back to the antenna with a loss corresponding to the tag's impedance and radiation change, which is affected by the crack under the tag. This difference between the transmitting and received powers is the backscatter power. Using the wave equation, backscatter power can be described as follows:

$$P_R = \frac{P_T(G_T G_R)}{4\pi}\left(\frac{\lambda}{(4\pi R_T R_R)^2}\right)^2 \sigma \qquad \textbf{(1)}$$

where P_R is the backscatter power (dB), P_T is the transmitted power (dB), G_T is the transmitting antenna gain (dB), G_R is the receiving antenna gain (dB), λ is the signal wavelength (m), R_T is the distance between the target (the RFID tag) and the transmitting antenna (m), R_R is the distance between the target and the receiving antenna (m), and σ is the targets radar cross section (m^2). If the transmitting antenna and the receiving antenna are the same, $R_T = R_R$. Since the backscatter power is in dB, and dB are unit-less, the backscatter power is a logarithmic way of describing the ratio between the power sent and received. This equation shows that reading distance affects

backscatter power. As this read distance increases by a quartic factor, the power is decreased. P_T can be determined using the received signal strength indicator (RSSI) logged by the reader equipment from the following equation. P_R can be determined using the RSSI logged by the reader equipment from the following equation:

$$\text{RSSI} = 10\log_{10}(\frac{P_R}{1\text{mW}}) \quad \textbf{(2)}$$

Where RSSI, which is in dBm (decibel milliwatts), is an expression of backscatter power. Most reading equipment uses a spectrum of reading frequencies. This changes the value of RSSI depending on the transmitting frequency channel. In North America, the signal frequency varies in the range of 902–928 MHz. The Impnj Speedway MultiReader software performs a hopping frequency data collection sequence in this range of frequencies during each collecting session. Through a MATLAB script, the gathered RSSI values can be averaged and the averages can be equally weighted across all frequency channels.

3.2.2 Volume-based Damage Extent

UHPC is a heterogeneous, cementitious composite material, with discontinuous fiber reinforcement, and a discontinuous pore structure (Russell and Graybeal, 2013). With these voids and reinforcements present, almost at random, the inner structure of this material can be less predictable than RC. Voids can appear within the first mm of the surface and the same goes for the reinforcement. For more realistic damage detection, a new index based on loss of volume was used. Usually, for visual inspection, especially for RC, cracks are measured in length and width (McGovern and Randall, 2001). However, to get a more complete idea of the crack, we

also measured the depth. Using a right triangular prism shape, the crack was idealized and able to be easily measured. Using the length, width, and depth of the crack, the volume index was obtained. This is shown in Figure 1.

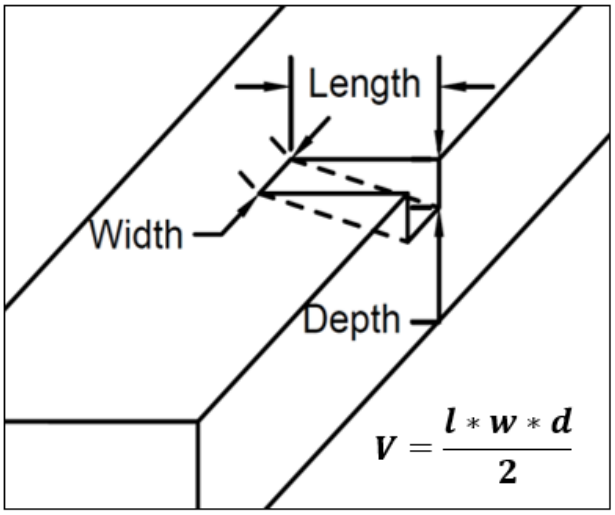

Figure 1: Crack dimensions**.** (Bruciati *et al.* 2019)

With this right triangular prism shape, the crack was idealized and not subject to the disorder of the material. This may not account for the voids that can appear in this material, but this index is superior in that it describes the three-dimensional nature of the crack.

3.2.3 Damage Index

Due to the nature of the hopping frequency data collection method, all data that is presented is in terms of mean RSSI. There are many ways to quantify this mean data. Two main ways are the actual value of the RSSI and comparison of two data states. These two data states would be the intact (RSSIi) state and the damaged state (RSSId). This index changes with each new damage stage. This will be referred to as the total damage index (TDI), shown as a percent (Martínez-Castro, *et al.* 2017). Thus, the total damage index is defined as:

$$TDI = \frac{RSSIi - RSSId}{RSSIi} \times 100 \quad \textbf{(3)}$$

where with the total damage index, crack identification and crack size changes can be correlated. When the total damage index value is a non-zero number, the crack volume has changed. The total damage index can take into account the non-uniformity of the tags. Due to the mass production of the RFID tags, no tag is perfectly identical. This characteristic would invalidate the use of the distinct values mean RSSI from each tag. Due to this, each tag reading needs to be compared to its own RSSI values by using the total damage index. If the tag is placed over the crack when the crack is in an early stage, it can be monitored. If the total damage index value is non-zero, then the crack volume has changed since tag's application.

3.3 Methodology

The UHPC specimen, sensor development, damage detection procedure, and experiment design are described in this section.

3.3.1 Specimen

Two UHPC specimens were fabricated for the experimental validations, UHPC with metal fibers (UHPC-A) and UHPC without metal fibers (UHPC-B). Both specimens have the same constitution and dimensions. The dimensions of the fabricated UHPC specimens are 1 inch

(2.54 cm) in depth, 2 inches (5.08 cm) in width, and 6 inches (15.24 cm) in length, as shown in Figure 2. The multiple cracks shown in Figure 2a are from the multiple tests done on each sample for this paper. UHPC-B has multiple cracks as well. The crack dimensions were different to ensure the range of the RFID tag. In Figure 2b, the metal fiber reinforcement is shown protruding from the sample.

(**a**)

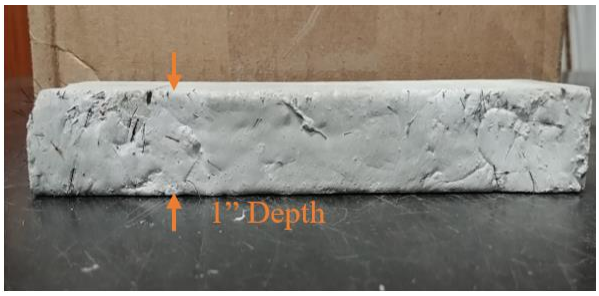

(**b**)

Figure 2: Ultra High-Performance Concrete Specimen with metal fibers (UHPC-A)**.** (**a**) Top view; (**b**) Side view. (Bruciati *et al*. 2019)

The specimen was a common commercial mix Ductal JS1212 (UHPC-A), produced by Lafarge North America (Ductal, 2017). The UHPC formulation contained premix power, water, Premia 150 (a modified phosphonate plasticizer), Optima 100 (a modified polycarboxylate high-range water reducing admixture), Turbocast 650A (a non-chloride accelerator), and steel fibers.

The steel fibers included in this mix design were non-deformed, cylindrical, high-tensile strength steel with a diameter of 0.008 in (0.2 mm) with a length of 0.5 in (12.7 mm). The steel tensile strength was specified as greater than 290 ksi (2000 MPa). The steel fibers had a thin brass coating providing lubrication during the drawing process and corrosion resistance for the raw fibers (Yuan and Graybeal, 2014). This metal working process was used for the reduction of the cross-section of the rod (Yuan and Graybeal, 2014). A steel fiber content of 2% by volume was used for UHPC-A. The composition of UHPC-A, by weight, is shown in Table 1.

Table 1: UHPC mix composition**.**

Components	**Amount (lb/yd^3)**	**Amount (kg/m^3)**
Premix Power	3700	2200
Water	219	130
Premia 150	30.0	18.0
Optima 100	20.0	12.0
Turbocast 650A	39.0	23.0
Steel Fibers (2%)	263	156

3.3.2 Damage Description

For the laboratory-scale validation, crack damage was simulated as a thin cut. The cut was made with a saw with a blade thickness of 0.03 inches (0.762 mm). Hasgul *et al*. (Hasgul, Turker, Birol, and Yavas, 2018), while studying failure modes, deflection/curvature ductility, and cracking patterns, used four-point bending tests to induce cracks in the UHPC. At the maximum strain, their UHPC experienced crack widths of 0.15 inches (3.8 mm). In this paper,

the crack width was simulated up to 0.08 inches (1.9 mm) in the first step. This width is similar to fatigue cracks shown after 20,000 cycles (Zhang and Bai, 2015), or cracks from forces such as temperature or shrinkage (Shim, 2005). The decision to attempt to match the smaller cracks mentioned previously was due to the likelihood of a crack of that size occurring. After 20,000 cycles, or shrinkage cracks are much more likely to occur than the maximum strain cracks created by Hasgul, due to the extreme circumstances that need to occur for maximum strain. The saw cut was very carefully made straight; however, the cut section could have chips and voids due to the intrinsic characteristics of the cementitious material. Saw cuts were made as uniform as possible, however, the crack volumes for each test could vary. This crack was simplified, as a representative of any cracks caused by bending, fatigue, or axial loads. The crack dimension was measured using a dial caliper that measures up to 10,000 thousandths of an inch from zero to six inches (0 to 15.24 cm).

3.3.3 RFID-Based Crack Sensors with Modifications for UHPC

The commercial UHF RFID tag used in this research was the Alien Technology ALN-9662 Short Inlay tag (Alien, 2019), as shown in Figure 3. This tag is EPG Gen 2 and ISO/IEC 18000-6C compliant and it uses a Higgs 3 EPC Class 1 Gen2 RFID tag integrated circuit (IC). The tag antenna is made of a flexible metallic material, which is adhered to a wet inlay. The cost for each dipole tag is about $0.10 for mass production. The antenna sensors can be fabricated on inexpensive substrate materials, such as paper, PVC (polyvinyl chloride), using low-cost fabrication techniques, such as inkjet printing (Zhang, *et al.*, 2017). This commercial tag is 70 mm long and uses a Higgs 3 EPC Class 1 Gen2 RFID tag integrated circuit (IC). Figure 3 shows

a detailed view of the IC and the tag mounted on the specimen. As shown, the antenna patch is oriented across the crack for test replicability and crack sensitivity uniformity. While this testing places the patch directly over the crack for test replicability and to ensure best possible crack sensitivity, the tag can still sense cracks not in that location as proved by Martinez-Castro. In addition, different than the previous study of crack detection on metallic surfaces by Martinez-Castro *et al*. (Martínez-Castro, 2018), the substrate between the tag and the specimen was removed. Therefore, direct tag attachment is feasible for crack detection on cementitious materials.

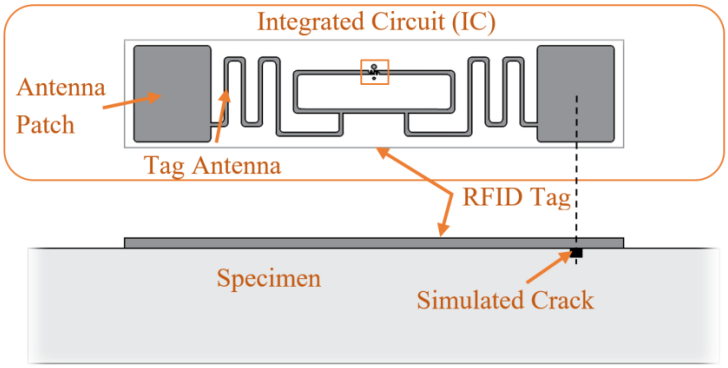

Figure 3: Commercial Radio Frequency Identification Tag**.** (Bruciati *et al.* 2019)

Because RSSI is affected by environmental factors near the sensor, sensor attachment methods should be identical at the different damage stages. The patch part of the tag was placed over the crack. The sensors were applied using 1 in x 0.25 in pieces of scotch tape, one on each corner. This secured the tag to the face of the specimen. The same application procedure was used for each tag, specimen and tested to ensure no other variables, besides the crack size, changed between each test. The attachment method was carefully tested via separate preliminary tests to control all the variables. This tag securing method is for trial uniformity, not to ensure the

capture of the extension of the concrete. Other factors such as radio wave reflection by the steel fibers and wall structures were kept constant. The testing was performed in a lab where these factors were able to be kept constant, as was the two systems identical reading setup/location for steel fiber effect minimization. In practice, this uniformity may not be possible if the structure has undergone repair since the tag was applied. The detailed logistics on sensor operation and replacement for field implementation is recommended. As the total damage index, which compares different damage states all with the same tag application, was used in all tests, the tape and other environmental changes had no effect on the results if kept constant.

3.3.4 Measurement Setup

The reflected power from the RFID tag was measured with two different systems, a lab-based system and a handheld system. The lab-based system consisted of a PC with Impnj MultiReader software connected to an Impnj Speedway Revolution R420 UHF RFID reader, shown in Figure 4a. A high gain circular right-hand polarized patch antenna was connected to the reader. Figure 4b shows the lab-based system setup at a read distance of 12 inches (88.9 cm).

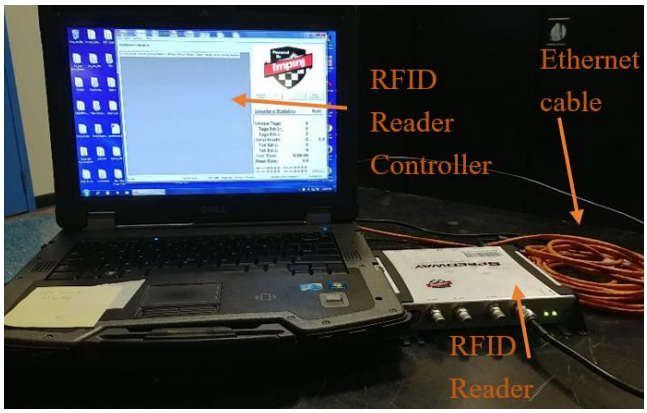

(**a**)

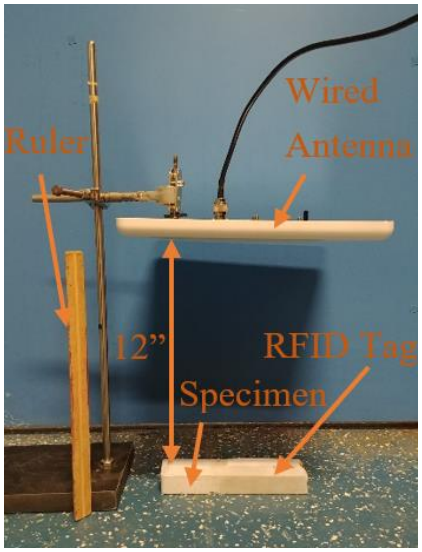

(**b**)

Figure 4: Lab-based system crack detection setup**,** (**a**) RFID controller and reader**;** (**b**) RFID specimen, tag and antenna**.** (Bruciati *et al.* 2019)

In a previous test the read distance of 35 inches (88.9 cm) was used. This was only for one test to confirm preliminary read-distance tests from the previous publication (Martínez-Castro, *et al.* 2017). The previous publication also confirmed the accuracy and usability of this setup. The setup was slightly varied for the other, smaller, read distances.

For data collection for the lab-based system, the MATLAB file averaged all the RSSI values from all the frequencies used by the antenna during the channel hopping sequence. It then displayed the mean RSSI value used in this study, as well as the unique identification for each tag. The lab-based system showed consistent damage identification performance in the past; however, it was lacking mobility for field implementation.

To improve mobility for field damage identification, another RFID reader with handheld functionality, i.e., ‘handheld system’, was employed. The handheld system used ATID AT870N PC RFID tag with a performance frequency of CE 850–968 MHz; 902–928 MHz are the frequencies used for North America. Using the Alien Handheld RFID reader app, the mean RSSI could be determined by a 1 Hz visual recording method, as the reader did not output a data file. The collected RSSI measurements were then averaged to create the mean RSSI. This system’s applicability was also tested as it was not tested in previous research. With acceptable performance that could overcome the difficulty in maintaining constant read distances, this system could be implemented in the field. This method will be referred to as the “handheld system” because of its mobility and field applicability. When compared to the lab-based system, the handheld’s ease of use is much higher. Without the need of any cables or a power source, because of being battery powered, if fully implemented, the superior crack monitoring system would be the handheld reader.

Figure 5: Handheld system**.**

The front attachment of the mobile PC is the UHF reader, shown in Figure 5. When the search for the RFID signal was initiated, the mean RSSI appeared on the screen along with the tag’s unique ID. Figure 6 shows the data collection setup for the handheld system with a read distance of 1 foot, which will be used for all handheld collection.

Figure 6: Handheld system crack detection setup**.** (Bruciati *et al.* 2019)

3.4 Experimental Validation

To validate the performance of the developed RFID-based crack sensors, a series of laboratory-scale tests were conducted.

3.4.1 Test 1: Read Distance Identification

To confirm the read distance of the RFID tag on the UHPC specimen, which increased, the antenna read distance of the mean RSSI value needed to be evaluated. Three tests were performed with various setups and readers. In the first test, four different tags and three different read distances per tag were examined. The three distances were 12 inches (30.48 cm), 24 inches (60.96 cm), and 35 inches (88.9 cm). These distances were chosen because, in Martinez-Castro's work, the distances were every 3 feet (91.44 cm). Therefore, one-foot (30.48 cm) intervals under three feet were untested. Due to each RFID tag having a unique backscatter power and the non-uniformities in mass production, four tags were used. These tags were then placed in the same location on the specimen for each read distance. The location was in a center vertical and center horizontal position (center–center) on the UHPC-B specimen. UHPC-B was used to minimize

the effect of the metal fibers on mean RSSI. Figure 7 displays the results of four different trials. In each trail, the mean RSSI value was read at three different distances. As expected, the value of the RSSI decreased as the read distance increased. This confirms the validity of this trend. Due to the quartic power reduction by distance, only one-foot intervals were investigated. Above three feet, the handheld system was unable to detect RSSI. Therefore, distances past three feet were not investigated, with one foot having the highest RSSI, this read distance will be used in the further experiments to sense changes in RSSI more clearly in both reading methods. This one-foot measurement distance is also feasible for field use. Being able to be within one foot of any location on the bridge is reasonable.

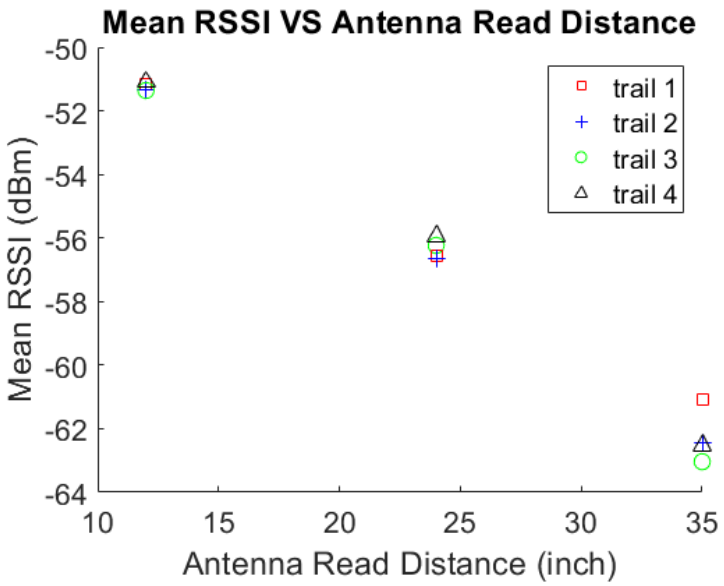

Figure 7: Mean RSSI vs. antenna read distance. (Bruciati *et al.* 2019)

3.4.2 Test 2: Crack Detection Using the Lab-Based System

The goal of Test 2 was to detect changes in mean RSSI with increased damage. Test 2 used only the lab-based system and tested UHPC-A and UHPC-B specimens. Test 2a used just UHPC-A with the lab-based system with three damage stages and the undamaged stage. Table 2

shows the increase in crack volume with respect to each damage stage and the total damage index. Figure 8 shows the corresponding graph. Studying the table, the trend of total damage increased with increased crack volume.

Table 2: Total damage index vs. crack volume: Test 2a.

Damage Stage	Crack Volume (in^3)	Crack Volume (m^3)	Total Damage Index (%)
1	0.00137	2.25×10^{-8}	0.00990
2	0.00252	4.13×10^{-8}	0.568
3	0.00303	4.97×10^{-8}	1.29

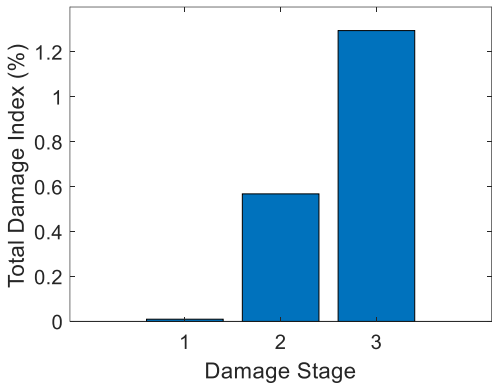

Figure 8: Total damage index vs. damage stage: Test 2a. (Bruciati *et al.* 2019)

Test 3 was crack detection using the lab-based system for UHPC-B, the specimen without metal fibers. The non-metallic reinforcement was the only thing that was different from the Test 2a. Again, the crack was simulated with different volumes with each damage stage. This test was to determine if the fibers heavily influenced the system. Figure 9 and Test 2b also yielded a positive trend of RSSI using the damage index. Test 2b showed that with the increase in the damage stage, which was an increase in crack volume, an increase of total damage index occurred**.**

Table 3 shows the results of Test 2b. Test 2b also yielded a positive trend of RSSI using the damage index. Test 2b showed that with the increase in the damage stage, which was an increase in crack volume, an increase of total damage index occurred.

Table 3: Total damage index vs. crack volume: Test 2b.

Damage Stage	**Crack Volume (in^3)**	**Crack Volume (m^3)**	**Total Damage Index (%)**
1	0.0000119	1.95×10^{-10}	0.177
2	0.00200	3.28×10^{-8}	1.06
3	0.00388	6.36×10^{-8}	1.18
4	0.00720	1.18×10^{-7}	1.25

In Figure 9, the tag had a positive trend with the largest increase being in Stages 1 and 2. This is because the crack volume was so small in Stage 1 as to be almost unrecognizable. The crack became significant in Stage 2; there was a large change in the radiation, which then increased the damage index. The change between damage stages may not have been as large in this test as in the previous but the trend still follows. Test 2b identified the effect of the metal fibers on the system. As predicted the metal fibers reflected more of the signal, as shown when comparing Stage 3 in Test 2a and Stages 3 and 4 in Test 2b. In Test 2b, Stages 3 and 4 had a higher crack volume than that of Stage 3 in Test 2a. Even with this higher volume, Stages 3 and 4 in Test 2b, which were without the metal fibers, had a lower total damage index than that of Stage 3 in Test 2a. The difference in the two tests was noticeable but not overly important as long as the crack could still be detected with or without the fibers.

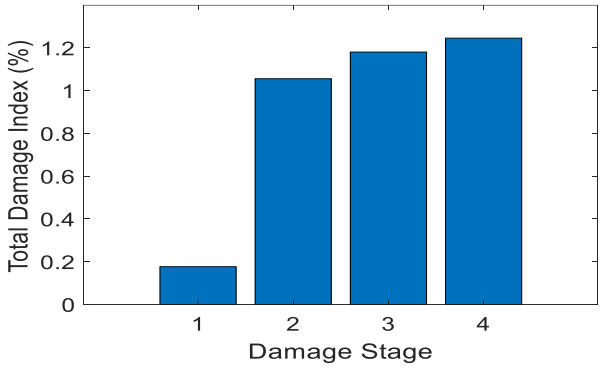

Figure 9: Total damage index vs. damage stage: Test 2b. (Bruciati *et al.* 2019)

3.4.3 Test 3: Crack Detection Using the Handheld System

Test 3 examined the performance of the handheld RFID crack detection system on UHPC-B, the specimen without metal fibers. The handheld system was used in the field as the inspector's tool for monitoring these cracks. In this test it was critical that the system identify the crack and its increasing volume. Table 4 shows the increase in crack volume with respect to damage stage and total damage index. Figure 10 displays the corresponding graph.

Table 4: Total damage index vs. crack volume: Test 3.

Damage Stage	Crack Volume (in^3)	Crack Volume (m^3)	Total Damage Index (%)	Standard Deviation
1	0.0000194	3.18×10^{-10}	0.60	0.297
2	0.000670	1.10×10^{-8}	1.88	0.316
3	0.00137	2.25×10^{-8}	2.68	0.297
4	0.00253	4.15×10^{-8}	2.63	0.346
5	0.00303	4.97×10^{-8}	2.75	0.453

Table 4 shows the crack volume per damage stage verses the TDI. As the damage stage and crack volume increase, the TDI does as well, the trend is better displayed in Figure 10. Figure 10 displays the positive trend of the total damage index while the damage stage increased. This was the same trend that Test 2 found with the lab-based system. However, the handheld test showed larger values for the total damage index. This could be because the non-uniformity of the UHPC material affected the readings differently with every crack. It could also be due to the handheld antenna having a higher power than the lab-based system, due to the lower strength signal sent or the wider range of data collection locations this system was designed for. The scale of these values is no more than double that of Test 2a. The tag, when used in a different location with data collected from a different reader, still performed as intended. As the crack volume increased, so did the total damage index. The standard deviation can also be examined in this test due to the collection method of the handheld reader. The first two damage stages have average standard deviations and they are also far enough away from the other TDI values from other damage stages to be examined

for significance. The last two stages have larger standard deviations which are believed to be due to the higher variation in radiation values coming from the larger crack.

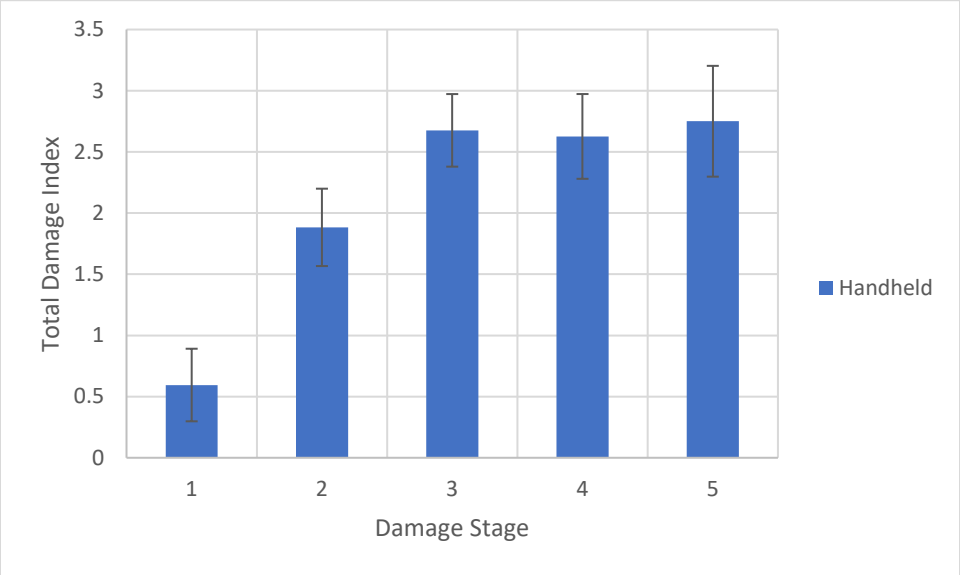

Figure 10: Total damage index vs. damage stage: Test 3.

At the last three damage stages the damage index changing very little. This is believed to be because the most change in the damage index happened at initial crack development. The index then tapered off, even as the crack got larger. The range of this tag was not tested past a maximum crack volume of 0.0072 in^3.

3.5 Conclusions

The RFID-based crack sensor was successfully used to monitor the increasing crack volume on UHPC. The crack volume range of this sensor has been confirmed to be from 0 to 0.0072 in3. This small range is due to the nature of the small cracks that UHPC develops. This low-cost commercial tags' performance was validated in lab-based experiments with two

different types of UHPC, with and without metal fibers, and two different systems (handheld and lab-based). The larger the total damage index, the larger the change in the volume of the crack since initial measurement. This development of a low-cost crack sensing system has great potential for the monitoring of new material, UHPC, where retrofitting has been done. This can improve the quality control of the retrofitting process and help inspectors expedite their work. Further work to validate the performance of the system in the field is underway.

CHAPTER 4. BWIM FULL-SCALE EXPERIMENTAL VALIDATION

In this chapter, information about the test span, the Meriden Bridge, will be described. These details include the bridge dimensions, traffic characteristics, and sensors implemented on the bridge. Also, the weigh station backed, previously collected data of four days and methodology behind the BWIM is introduced. The results of GVW accuracy and speed calculation based on the previously mentioned methodology is presented.

4.1 BWIM Test Span: Meriden Bridge

The bridge used in this study is bridge number 03051, located in Meriden Connecticut, the location is shown in more detail in Figure 11 and Figure 12. It carries three lanes of Interstate 91 (I-91) Northbound over Baldwin Avenue. The bridge has a total length of 85 ft., a width of 55ft. and a bridge skew of 11.5˚.

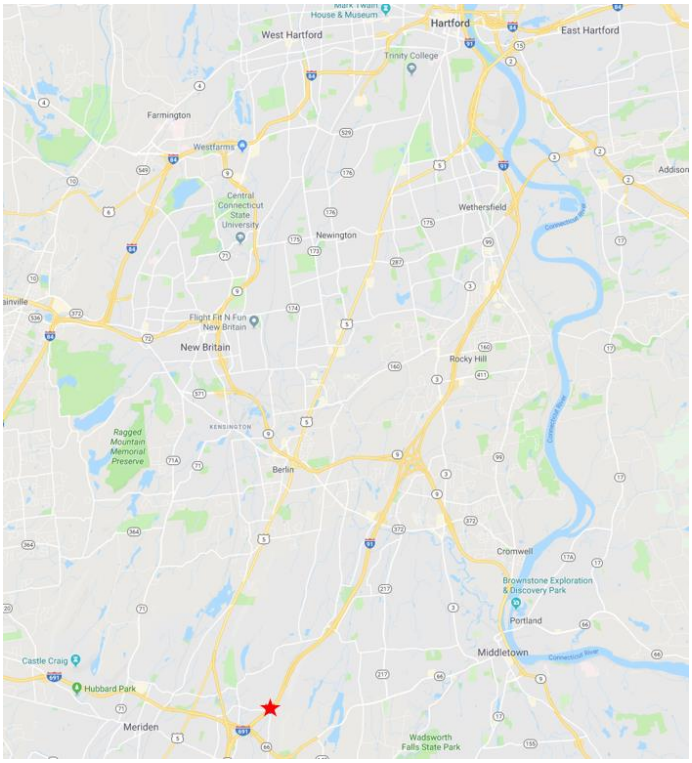

Figure 11: Map view of Meriden Bridge *(Google Maps, 2019)*

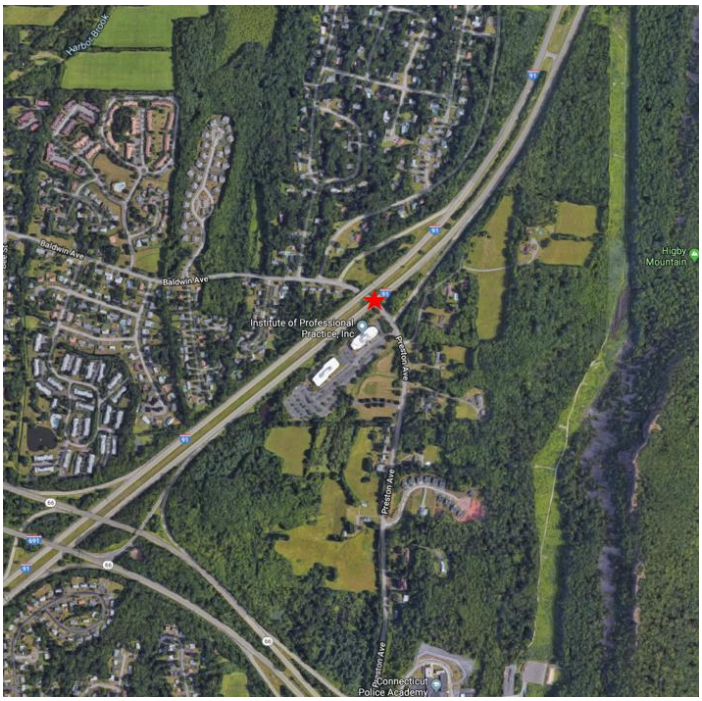

Figure 12: Satellite View of Meriden Bridge *(Google Maps, 2019)*

Previously mentioned, COST323 has recommended parameters for ideal candidates for BWIM systems. The bridge length falls into the recommended category and the skew is in the acceptable zone. According to the 2017 National Bridge Inventory (NBI), the average daily traffic (ADT) of the bridge is 57350 and the percentage of trucks is 14%. Making the average daily trucks loading of 8029 times (FHWA, 2017). Shown in Figure *13* is the west elevation of the bridge.

Figure 13: West Elevation of Meriden Bridge

According to the NBI, the bridge received a bridge rating of a "6" which corresponds to a "Satisfactory Condition" rating from the CTDOT Bridge Inspection Manual (McGovern and Randall, 2001). This rating indicates that the overlay is also at least in "Satisfactory" condition. This fits into the acceptable class 3 acceptable for pavement characteristics in COST 323. The bridge could be in a lower class such as 2 Good, but the deflections and requirements asked for are not obtainable for this study. Figure 14 shows the dimensions of the bridge.

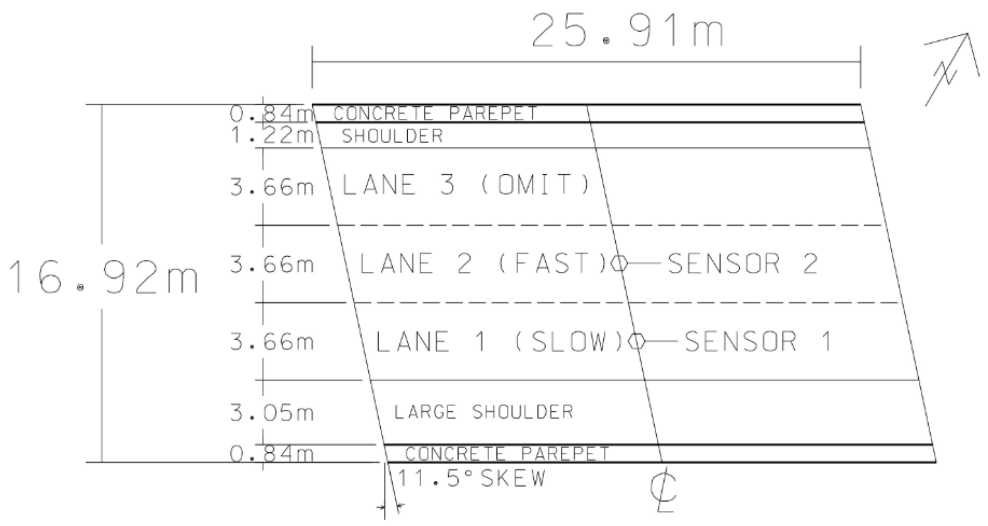

Figure 14: Meriden Bridge Plan View (Wall, *et al.*, 2009)

In Figure 14 there are three lanes shown. Lane three is the far-left lane, as trucks are not allowed to travel in this lane, this lane is omitted from study. The middle lane is considered "fast" because this would be a lane that trucks would use to pass other vehicles that are in the slow lane. Therefore, going faster than the slow lane. Lastly, the slow lane, which is basically the most often lane trucks are found in and travel the slowest when compared to the other lanes. Sensor 1 and sensor 2 are the strain sensors used in this study. They are on the underside of a girder and these girders are located about under the center of each lane respectively. For reference of all the data used in this study is shown in Figure 15. From this figure, it can be shown the total number of vehicles known weights available for this study. The total is 221 known weights, but the system still calculated the weights of vehicles with unknown weights and the entire total is 324 calculated weights. This 324 is only for the strain-based methods that will be explained later in this paper.

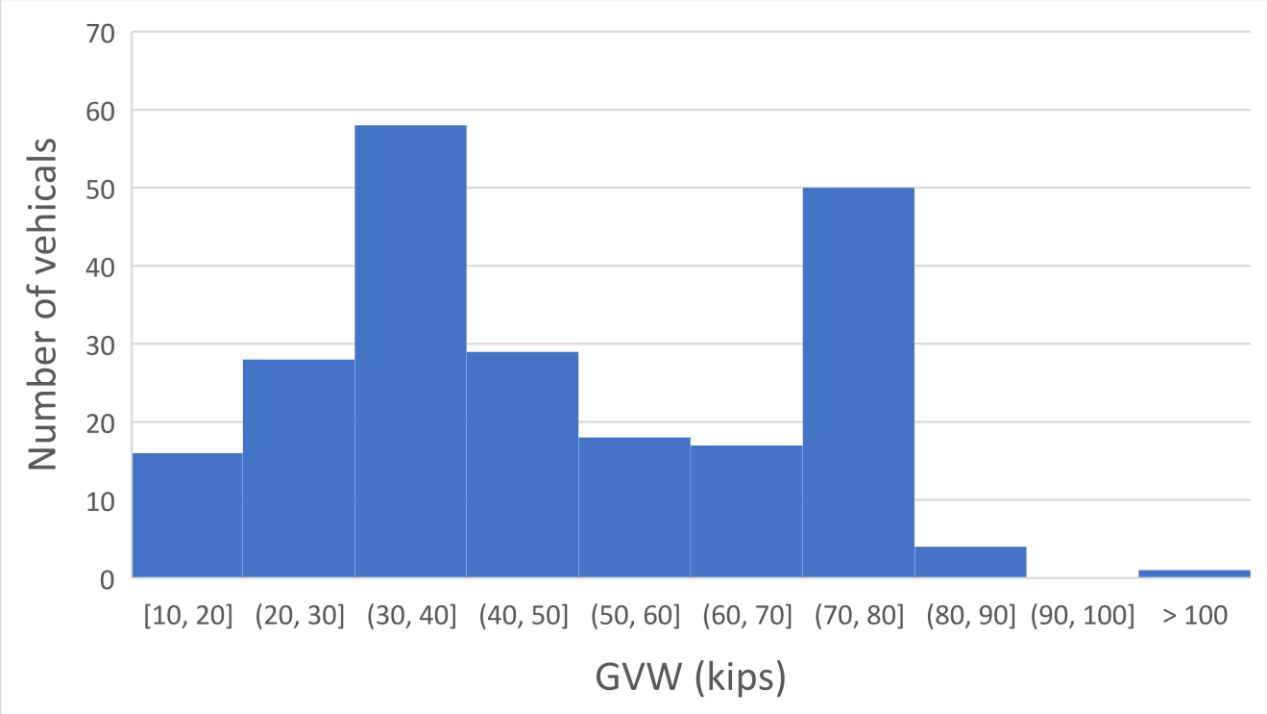

Figure 15: Entire database of weigh station weighed vehicles and their weights.

4.2 SHM-BWIM System

A dual SHM and BWIM system has been installed on the Meriden Bridge. 38 sensors total have been installed on the bridge. This includes 18 foil strain sensors, 4 high sensitivity quartz strain transducers, 8 piezoelectric accelerometers, 4 capacitive accelerometers, 4 resistance temperature detectors, and one microphone (Kolev, 2015). On Figure 17 these various sensors and locations are shown.

The data acquisition (DAQ) system setup is a national instruments (NI) NI cDAQ-9178 CompactDAQ chassis with four different types of modules for different types of sensors. The chassis is connected to a Dell Ultra Small Factor-Optiplex 780 desktop using a USD 2.0 cable. Matlab is used for the data analysis and collection. All the DAQ system components are stored in

a converted traffic signal cabinet underneath the south abutment of the bridge shown in Figure 16.

Figure 16: Cabinet housing system underneath Meriden Bridge *(Li, 2014)*

For this study, out of the many piezoelectric strain sensors used, only 2 of them, located in the center of girders 4 and 6, were used. Both sensors were installed on the web of the girder, just above the bottom flange to measure vertical strain (Kolev, 2015). Girder 6 and 4 are located directly under the slow lane and middle or "Fast" lane respectively. This bridge has three lanes total, but very few trucks are known to travel in the far-left lane, which is why the lane 3 label is titled "Omit". As a result, data was not collected from the omitted lane. The girders were expected to have the highest strain measurements at midspan, which is why the sensors were placed there. The middle lane will be referred to as lane 2 and the slow lane will be referred to as the slow or lane 1.

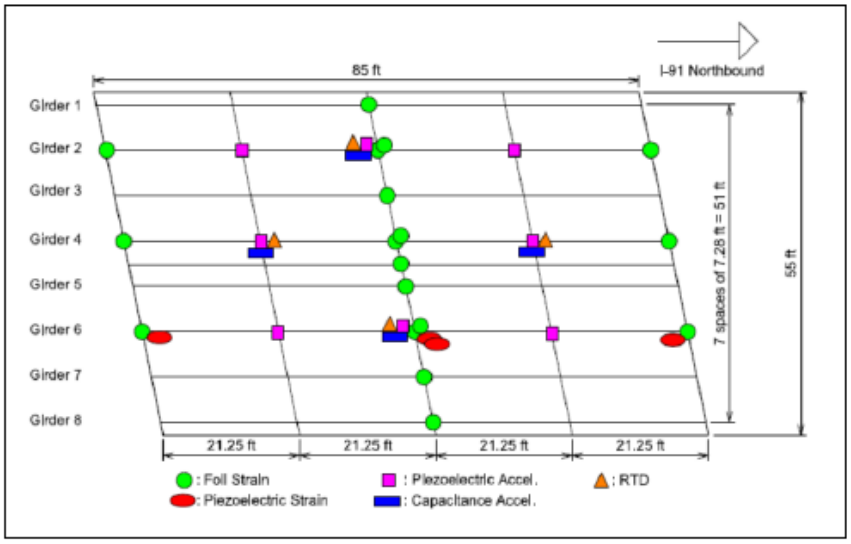

Figure 17: Schematic of sensor layout and types (Christenson *et al*. 2012)

All data collection, sensor use, and sensor installation was performed in previous studies. No actual field work was done for this research. The data was collected during three days in 2013 and one day in 2015.

4.3 BWIM Methodology

This study uses one strain sensor per traffic lane to obtain the strain time histories that are used in the speed and GVW calculation of trucks passing over the instrumented bridge. Both sensors are located on the underside of the flange of the steel girders of the bridge and their locations can be seen on Figure 14. These measure the vibration excitations of that specific girder, which is located under a travel lane.

The developed theory uses the assumption that each girder under a lane behaves as a simply supported beam when exposed to a load from that specific lane. The Meriden Bridge's girder layout has a girder directly under each highway lane. Each axle or axle group of a vehicle

can be assumed to act as a point load moving along the girder at a fixed spacing and a constant speed. This will make the vibration response caused by each moving truck to act like a group of point loads moving along a simply supported beam.

The GVW is found by relating a known GVW from a calibration vehicle to the unknown GVW of the unknown vehicle. This method was developed by Ojio and Yamada (2002), and was used by Wall (2009). The GVW of an unknown truck can be determined by multiplying the influence area of an unknown truck by a calibration factor. The influence area, A, of a single truck that has passed over the bridge is defined as equation 4 and this area can be modified be with respect to time, by multiplying it by speed shown by equation 5.

$$A(x) = \int_{-\infty}^{\infty} \varepsilon(x)dx \quad \textbf{(4)}$$

$$A(x) = v \int_{-\infty}^{\infty} \varepsilon(t)dt \quad \textbf{(5)}$$

Where ε is the response is wave and x_n is the distance between the axels. The response wave is the strain response from the vehicle traveling over the bridge. This can be defined as the strain at a specific point of the bridge due to the multiple moving point loads.

$$\varepsilon(x) = \sum_{n=1}^{N} P_n f\,(x - x_n) \quad \textbf{(6)}$$

Where P_n is the weight of the nth axle and $f(x - x_n)$ is the influence line of a simply supported beam. This is defined as:

$$f(x) = \begin{cases} \frac{cx}{2EI}, & 0 < x < \frac{L}{2} \\ \frac{cL}{2EI}\left(1 - \frac{x}{L}\right), & \frac{L}{2} < x < L \end{cases} \quad \textbf{(7)}$$

Recognizing that the GVW is the summation of the moving point loads, the GVW can be defined as:

$$GVW = \sum_{n=1}^{N} P_n \quad \textbf{(8)}$$

With the GVW and the influence area determined, the ratio of the known areas and weights to the unknown can be applied. With every bridge having slight differences a calibration factor is implemented. The constant is defined as:

$$\beta = \frac{GVW_k}{A_k} \quad \textbf{(9)}$$

The subscript k indicates a known value. The beta can be calibrated using a known GVW of a truck passive over the bridge and its corresponding influence area. This relationship can also be applied to the unknown values which involve the subscript u.

$$GVW_u = A_u\beta \quad \textbf{(10)}$$

these terms, the substitution can be made and the relationship between unknown and known can be shown as (Wall, 2009).

$$\frac{Ak}{GVWk} = \frac{Au}{GVWu} \quad \textbf{(11)}$$

Where, $GVWk$ and $GVWu$ are GVW weights of known and unknown trucks, and Ak and Au are influence areas for known and unknown trucks, respectively.

Finally, the strain can be represented over discrete time intervals, as shown

$$A_u(x) = \frac{v\Delta t}{N}\sum_{i=1}^{N}\varepsilon(i\Delta t) = v\int_{-\infty}^{\infty}\varepsilon(t)dt \quad \textbf{(12)}$$

Where, Δt is the discrete time interval, and N is the total number of measurements needed for the truck to cross the bridge. The method of Ojio and Yamanda (2002) does not account for the dynamic effects of the bridge response in its calculation of GVW.

Speed calculation of the vehicle is an essential piece in determining the vehicles GVW. In Equation 10 the beta is defined by Equation 9 which contains two know variables. The Au is defined Equation 12. While the strain response is gathered from sensors, the velocity is unknown. Using the bridge response, this paper uses 3 ways to estimate the speed of the vehicle.

4.4 Speed Calculation

The speed of the traveling vehicle is essential in this BWIM algorithm. The two ways used to calculate the vehicle speed are outlined next.

Method 1: Backside strain-based approach

The first is a more popular method and that is using the end of the strain time history curve (Kolev, 2015). The goal is to capture when the last axle of the truck is over midspan of the bridge and when the last axle is leaving the bridge. This will be referred to as “Backside Strain Time History (STH)”. This method, as with all the other methods, separates each truck passing as a separate truck event. The MATLAB code will analyze each event separately. For the Backside STH, the strain of the bridge girder will have already experienced the max strain caused by the vehicle and will be returning back to zero, or whatever the residual strain will be, including measurement noise. An example of this backside STH curve is shown in Figure 18.

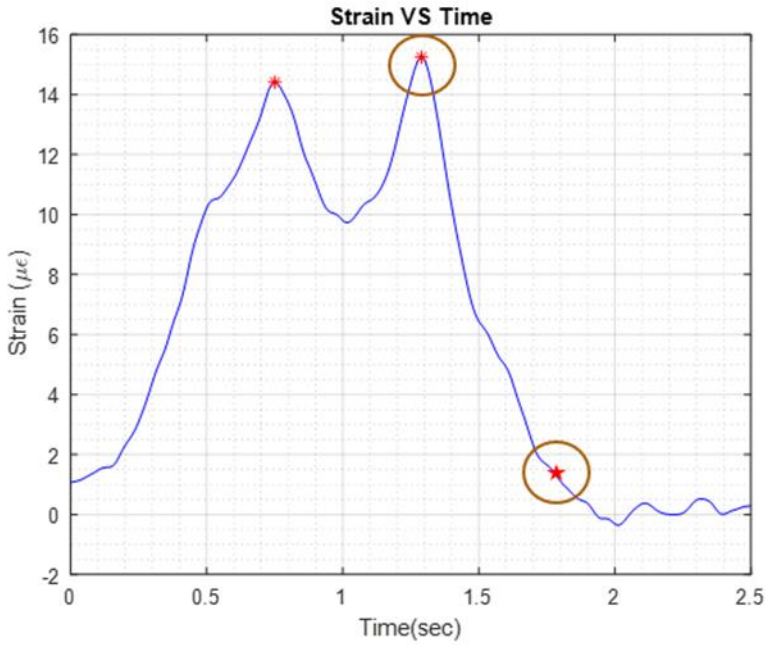

Figure 18: Backside STH

The MATLAB algorithm identified two peaks, both above 14 microstrain. The second peak is the rear peak and will be used in this method. To obtain the speed, the time from the last peak, which is due to the last axel of the truck passing the midspan of the bridge, to the time of the "no peak", which is when the truck leaves the vehicle is calculated. "No peak" here is 11% of the max peak value. This is because the strain value, most of the time, never actually reaches a zero value because of measurement noise, other vehicles, or continued vibration of the bridge. This 11% is used to be ideal for this data set and can be improved with more data or machine learning algorithms, discussed in future work, to obtain a universal value. For this data set however, the 11% perforated optimally when compared to 5 other percentages which range from 7 to 12 in 1 percentage intervals. Once the time from the two points is obtained, because the distance from mid span to end span is known, 42.5 ft, the speed can be calculated and then used in the

previously mentioned methodology. The results for this particular truck event are listed in Table 5.

Table 5: Backside STH event results

Screen GVW	Calculated GVW	% Difference	Speed (MPH)
62.64	64.37	2.76	56.24

The screen GVW corresponds to what the screen displayed at the weight station. This mean that this is the actual GVW of the vehicle. The calculated GVW is what the algorithm calculated and the %difference and Speed are self-explanatory; speed was also calculated.

Method 2: Frontside strain-based approach

The second speed calculation technique uses the front side of the STH. This will be referred to as "Front side STH". As the previous speed calculation method, the time from a peak to a "zero value" is calculated and then the speed is found. This correlates to when the first axle enters the bridge to when the first axle reaches midspan of the bridge (Wall, 2009). Shown in Figure 19 is the Frontside STH.

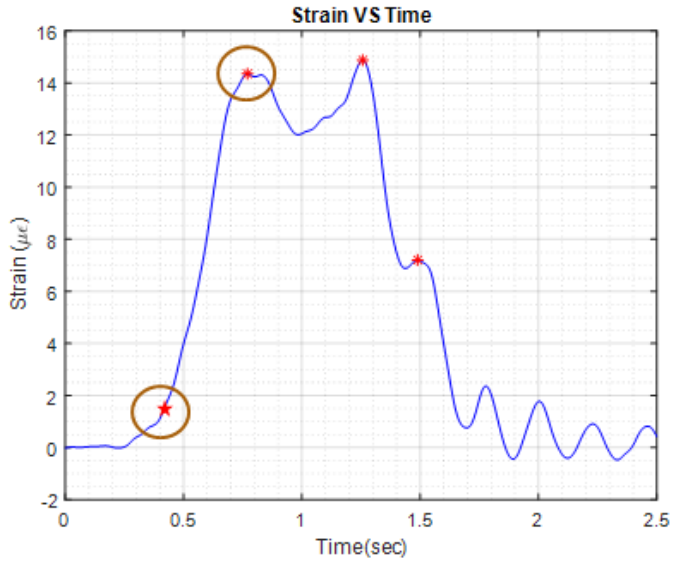

Figure 19: Frontside STH

The reason this method differs from the backside STH method is due to the residual vibrations that can occur. After 1.5 seconds in Figure 19 there is a oscillating strain pattern. This pattern is assumed to be the bridge vibrating due to the truck unloading. When this occurs, as this does not always, the frontside STH is the method to use because the backside STH method will incorrectly identify peaks and therefore, not calculate the speed correctly. This method also uses the 11% for the "zero value".

Table 6:Frontside STH event results

Screen GVW	Calculated GVW	% Difference	Speed (MPH)
72.84	75.13	1.41	74.7

The percent different between the frontside and backside show that the algorithm guessed the GVW more accurately in the frontside event. That is not always the case; both methods have events that are easily calculated either way.

A common assumption of these two methods is that what if the front and back of the STH makes it difficult for the algorithm to calculate the speed. Shown in Figure 20 is an example of where the frontside and backside STH cannot calculate the speed correctly.

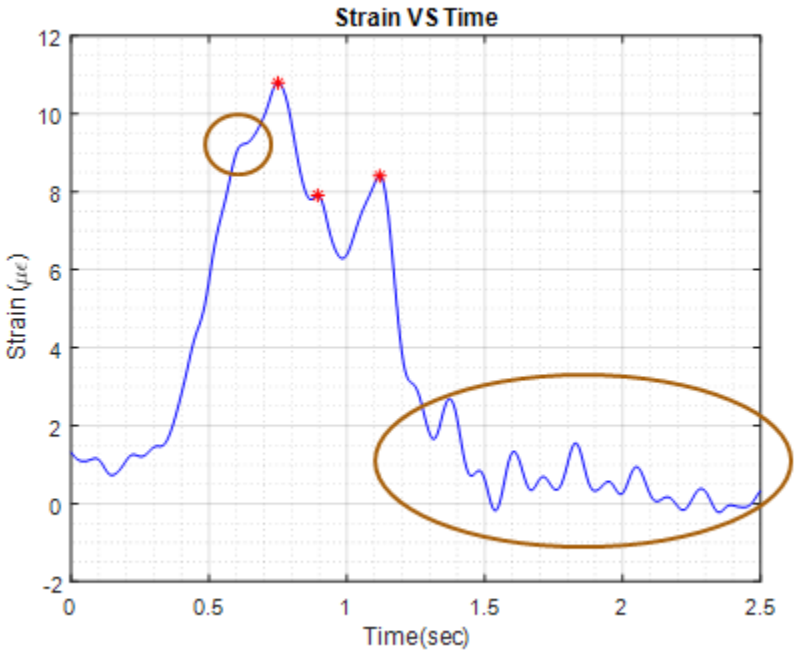

Figure 20: "Unfavorable" nature of a STH truck event

The first unfavorable nature of this STH is in the first brown circle at around 0.5 seconds. Here the peak was not identified by the MATLAB code. This peak is assumed to be the first set of axles on the truck and because it was not identified, the frontside STH method GVW calculation was incorrect. The second brown circle centered at around 1.75 seconds is about the vibrations after the truck passes over the bridge. This was explained previously during the

frontside STH discussion, but is mainly due to other vehicles, noise, or continued vibration by the bridge from the truck loading. When the first two methods have high error results, the third method can sometimes pin point the speed.

4.5 Calibration Coefficient, Beta

Before the results of the algorithm refinement are discussed, the value of the calibration coefficient, beta shown in equation 9, needs to be explained in more detail. In equation 9, it shows how to calculate beta. The GVW known and A known are needed. This is obtained, for this research, by calibration truck. In December of 2010, previous researchers from the University of Connecticut used a 5 axle, 68,360 lb truck for this vehicle (Kolev, 2015). The truck had a length of 68 ft. and made multiple passes over the bridge. The truck made passes over lanes 1 and 2 a total of 11 and 5 times, respectively. For each of the trials, the truck was moving at a constant speed varying between 47 and 63 mph. The strain response was then matched with each trial. With the GVW, speed, and strain response known, equation 9 can then calculate beta. The calibration truck used in December is shown below.

Figure 21: Calibration truck used in December 2010 *(Kolev, 2015)*.

During the calibration, the optimal beta value for each lane was determined using trial and error and equation 9**.** For this research, beta for lane 1 is 0.03876 and beta for lane 2 is 0.035394. These values were determined in previous research. As the goal of this research is not determining new beta values or studying how the beta value will change from 2010 to 2013 and 2015, the assumption is the beta value is correct/optimized. Another way that the beta value can affect the results and having a bias towards the calibration vehicle. This bias would make it so trucks of the same type as the calibration vehicle would have their GVW calculated more accurate and more often than all other vehicles. In an ideal world, there would be many different types of calibration vehicles, all making many passes at different speeds and weight distributions. Due to budget and time constraints however, this is not possible. This bias was noticed in the results, but not significant enough to skew any conclusions, so just a mention of it was needed.

4.6 Results

As shown before in Figure 15, there is a total of 221 known vehicle weights. With this in mind, the calculated weights, which show these known weight cases and also unknown weight cases, are the be presented in this section. The calculated speeds, which play a large role in the weight calculation, are also to be shown here. The speeds however, have no known speeds to be compared to due to the experimental setup in which the data was collected in previous research.

Before the BWIM results are shown, the calibration of the 11% of peak strain value, used in the speed calculation section, can be shown here. Previous work from researchers such as Lobo-Aguilar (Lobo-Aguilar, 2018) use a percentage of the max strain to calculate the speed. As

mentioned previously, this value is used to minimized the effects of noise and vibration in the sensors. A total of 6 different values were tested. The methodology behind these values are gathered from characteristics of this data set. These noise and vibration effects can reach up to 50% of the maximum strain as seen in figure 19 which has a false peak at 1.5 seconds. A trend was noticed during analysis that shows average effects of about 10% of max strain. While other BWIM refinement methods discarded many of these effects, some still remained. This 10% was used as a starting point to determine a unique value for this data set. Shown below in table 7 is the results of this analysis. Percentages in 1 percent intervals were tested from 7 to 12 percent. Once the value of 11% was tested, the other values outside of 11% started to diverge, and thus 11% was used.

Table 7: Determination of "Percentage of Peak Strain" Value

Percentage of Maximum Strain (%)	**GVW Error Percentage (%)**
7	11.54
8	10.50
9	10.41
10	9.67
11	8.83
12	9.40

Now that the methodology refinement results are presented, the BWIM results can be shown.

First, the calculated speed for each method will be presented. As said before, the speeds accuracy has a large impact on the accuracy of the GVW. The first figure to be presented is the speed calculation distribution of method 1. Without the errors method 1 has a 39% of calculated speed within 5 mph and a 79% within 15 mph. COST 323 has a criterion for grading the speed calculation portion of GVW calculation, but because the actual speeds are unknown, this average is used. Here, only 14 time were the speeds calculated 25 mph or more away from the average. Method 2 and 3 will be presented without the histogram with errors, but otherwise will be uniform.

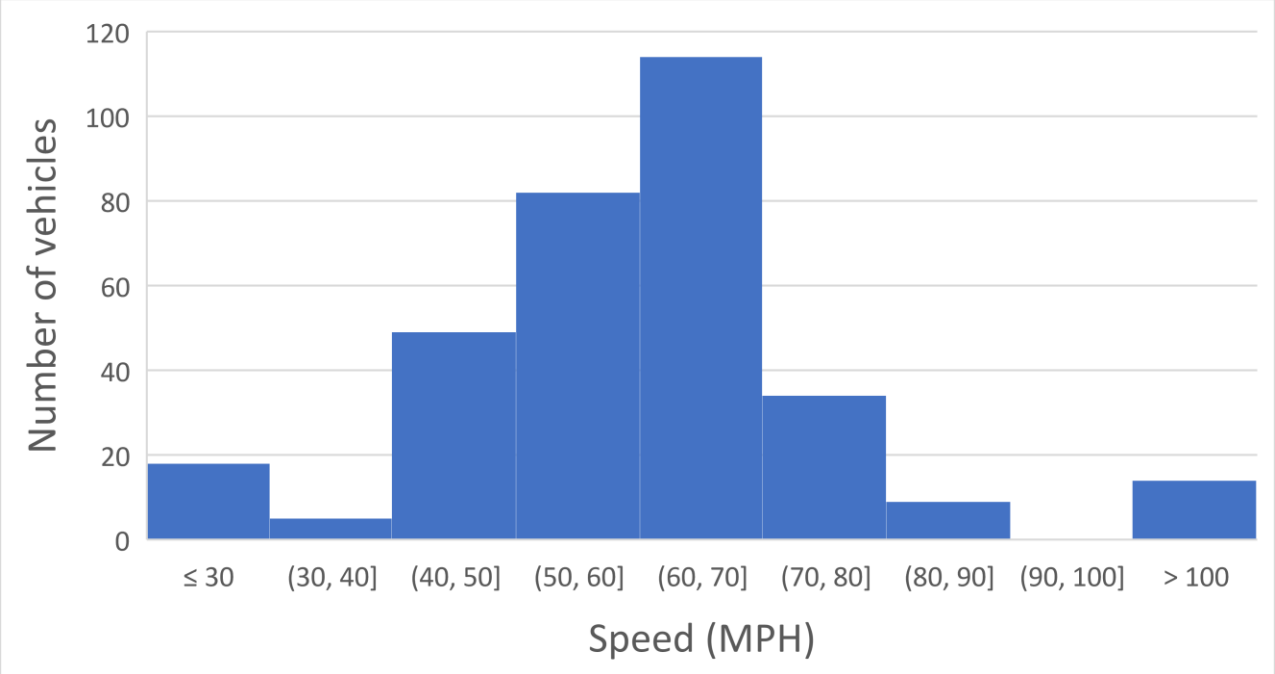

Figure 22: Method 1 calculated speed distribution.

With the second evaluation, both percent ranges increase and this can be seen in Figure *23*. The amount of speeds calculated that are outside the 30 and 90 range are zero because of the way the algorithm is defined. It understands that these calculations were errors.

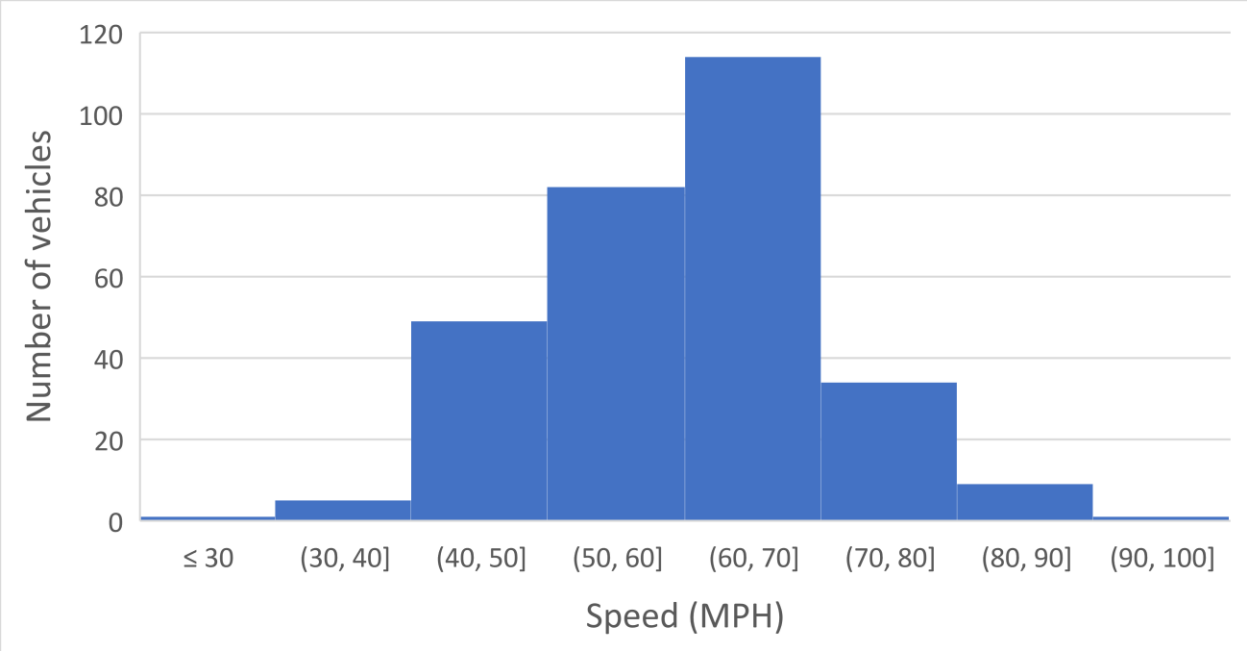

Figure 23: Method 1 calculated speed distribution with errors removed.

Method 2 uses the same idea as method 1, but uses the frontside of the strain plot. The first evaluation, which pertains to the "with errors" distribution, also showed promising results for accurate speed calculation. For the 5-mph range away from the 65-mph average, method two shows 20% of the speeds in that range. For the ±15 mph range, 57% of the speeds are inside that range. These numbers are both below method 1's percentages, but this is still a valid alternative to method 1 when it cannot be done accurately. Another thing to notice is how this method creates less errors than method 1. Method 1 had 32 trucks over 100 or under 30 mph, while method 2 had only 21 trucks outside those values. Next, without the errors, which is shown in Figure *24*. With the errors removed, the second evaluation can be done. The ±5 mph range increased to 22% and the ±15 mph range increased to 61%. These increases from the first evaluation to the second are smaller due to the lesser amount of errors method 2 creates. Regardless, both values still increased.

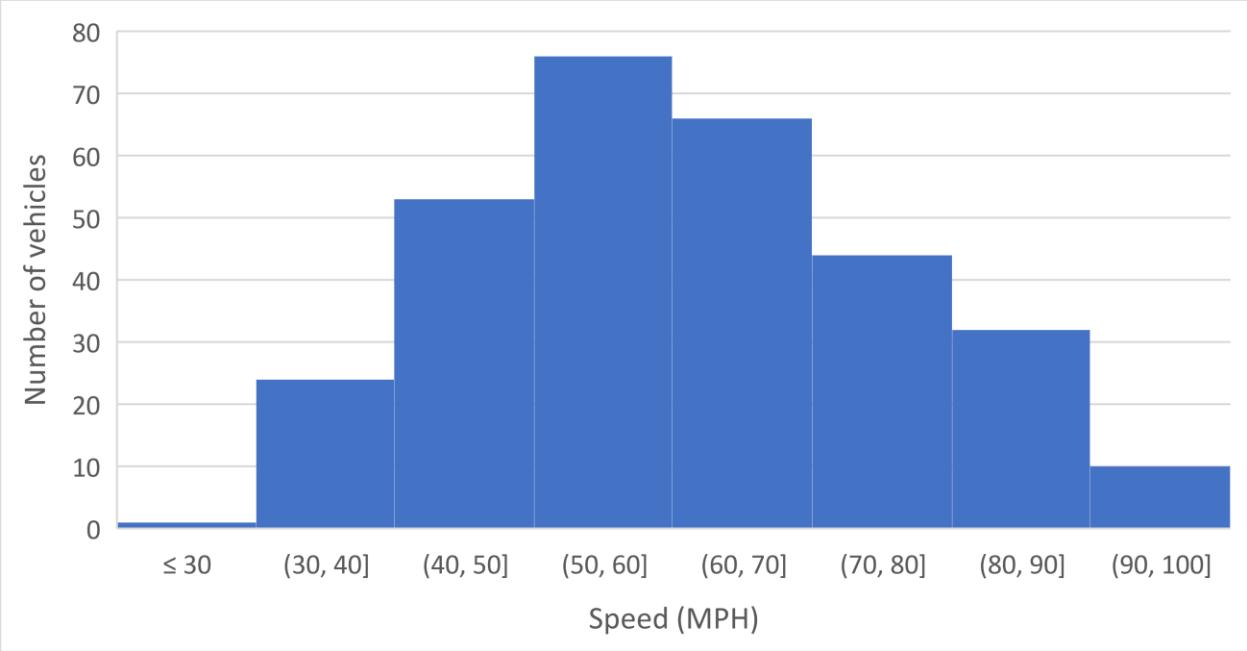

Figure 24: Method 2 calculated speed distribution with errors removed.

Next the GVW distributions and accuracies will be evaluated. The GVW's will all be examined with the data when the speed was calculated over 100 or under 30 mph removed. This is done because when the algorithm calculates a speed outside that range, it assumes it calculated the speed incorrectly and rather than calculate the GVW anyway, it does not because it will most likely be incorrect. The characteristics of highway traveling trucks has a very low chance to be traveling outside this range which is why the algorithm assumes it is incorrect. While the range from 30 to 100 can be changed, the author feels that this will represent the quality of the algorithm the best without skewing the results by reducing the data size by a larger quantity; also, the 30mph and 100mph are unlikely speeds, but can happen. For each method two graphs will be shown. The first will be the distributions of the GVW's calculated. This can be compared

to Figure 21 as an estimate of how accurate the method is. The second graph will show the exact percent difference of each trucks weight compared to the calculated weight. In accordance with COST 323 the method will be given an accuracy class dependent on confidence intervals. For example, accuracy class A(5) needs to have a confidence interval width of 5% (COST 323, 2002). Class B+(7) needs to have a width of 7% and so on. This means that 95% of the truck weights need to fall within this percentage error to be placed in that class. The method will then be given another grade based on the tolerance interval, but with a larger 85% interval as use in other research (Lobo-Aguilar, 2018).

4.6.1 Method 1. Backside Strain-Based Approach:

Method 1's performance of GVW calculation will be first. As shown in Figure 25 the distribution of the GVW are shown. Right below the GVW are the % differences distribution between the known GVW in Figure 26. When comparing Figure 25 to Figure 15 a trend can be noticed. Both figures have higher volumes of vehicles in the 30-40 and 70-80 kips range. One specific thing to note is method 1 did not estimate any weight close to 146 kips, which is the highest weight recorded in these data sets. This is due to the immense load creating much vibration in the bridge and making the strain plot difficult to use for thus algorithms aim. It is also due to the vehicle traveling very slowly, which makes the end of the strain plot outside of the designated window for normal speed vehicles, which is what this research is aimed at. Moving on to Figure 26, it can be seen that 45% of the vehicles were within 10% of the actual weight. For an 80-kip truck, the maximum non permit truck in CT, that's a max of only 8 kips off for the worse case of 10% off. Using the COST 323 guidelines, the grade given to this would be D(25)**.** For a method that only uses 1 under the bridge sensor, this shows great promise when compared to other systems. With the next grade being given to this system when it expands the

5% error to 15%, the grade given is D+(20). The D+(20) grade system can be used for "detailed statistical studies, determination of load histograms with class width of one or two tonnes, and accurate classification of vehicles based on the loads; as well as infrastructure studies and fatigue assessments" (COST 323, 2002). The D(25) can be used for "weight indications required for statistical purposes, economic and technical studies, standard classification of vehicles according to wide weight classes (by 5 tonnes (11 kips)).

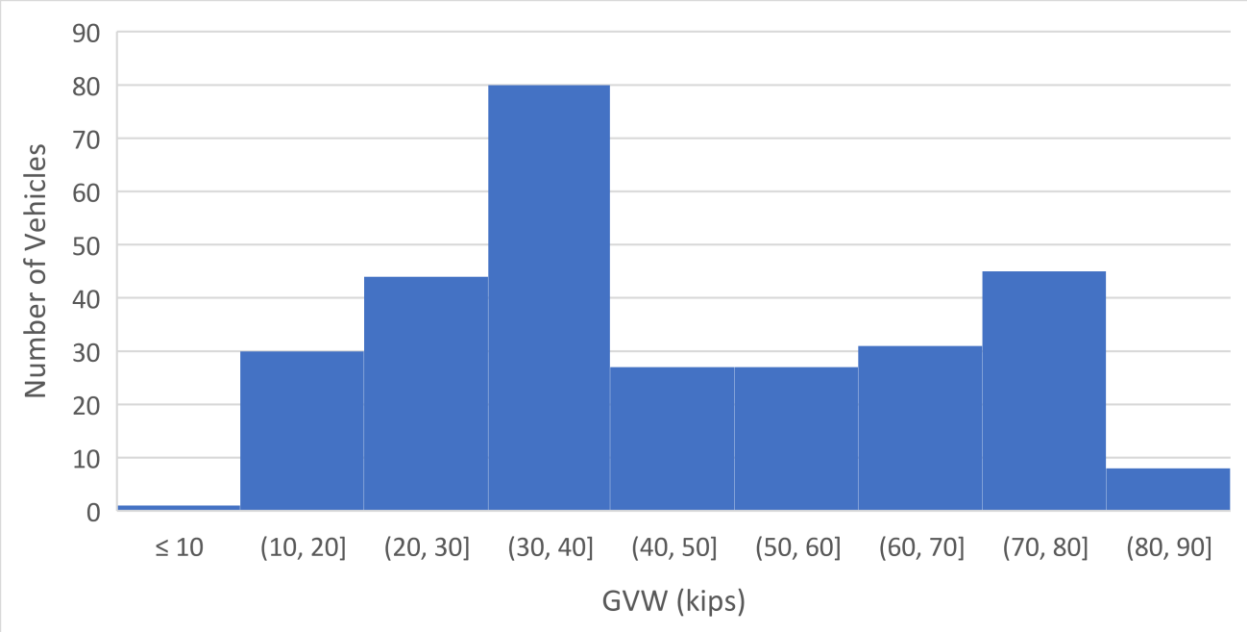

Figure 25: GVW distribution of method 1.

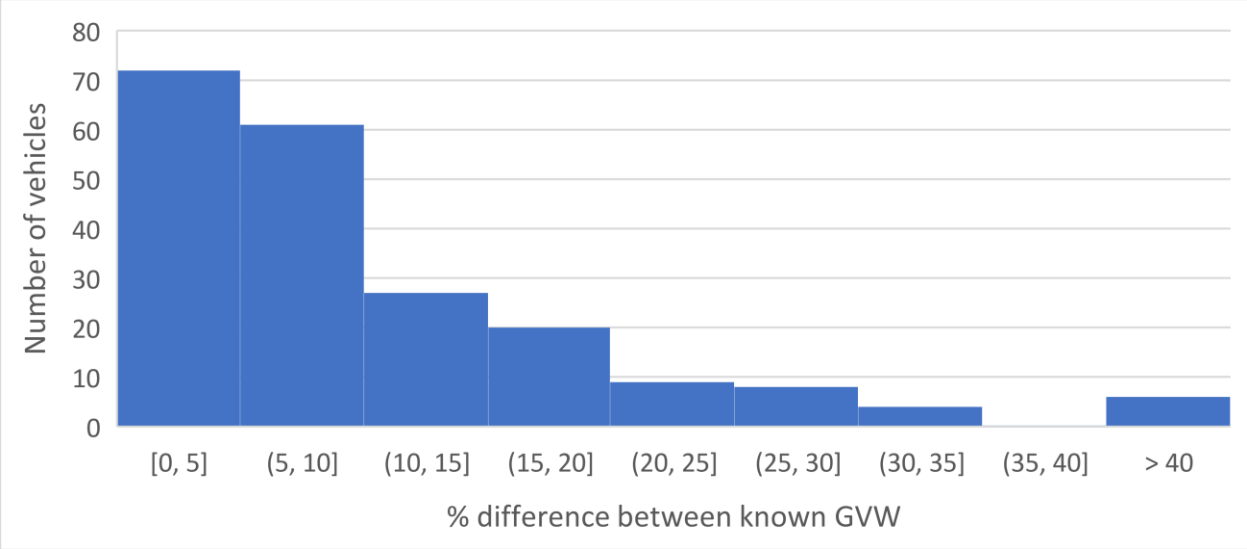

Figure 26: Percent difference between known GVWs of method 1.

4.6.2 Method 2. Frontside Strain-Based Approach:

Method 2 GVWs performance evaluation is next. Shown in the two figures below are the same figure characteristics as method 1, but with method 2's data. Like with the previous method, Figure 27 can be compared to Figure 15, which shows the actual GVW distribution. The 30-40 kip range of trucks has about the same number of vehicles in each figure, only about 2 vehicles difference. The 70-80 kip range however, is lower by 13 vehicles than that of Figure 15s. The 60-70 kip range has about a 20 vehicle difference, but this is due to many vehicles weighing about 80 kip, the legal permit less limit in Connecticut, so many vehicles are close to that 70-80 range and were slightly miscalculated, but still fall into the higher range. Otherwise, all the other columns trends are similar, even the 100+ kip column has the 1 truck. With Figure 28, the COST 323 guidelines come in to give a grade. Unfortunately, there is a large number of vehicles that have been estimated to be over 40% off from their real values. This means the COST 323 grade is an E(45) after expanding the graph to see the extent of the over 40 category.

With the change from the 5% from COST 323 to 15% from previous research, the grade is improved to just barely a D(25). Classes of E grade are defined from systems which do not meet the grade D(25) requirements. These systems are useful to give indication about the traffic composition and the load distribution and frequency (COST 323, 2002).

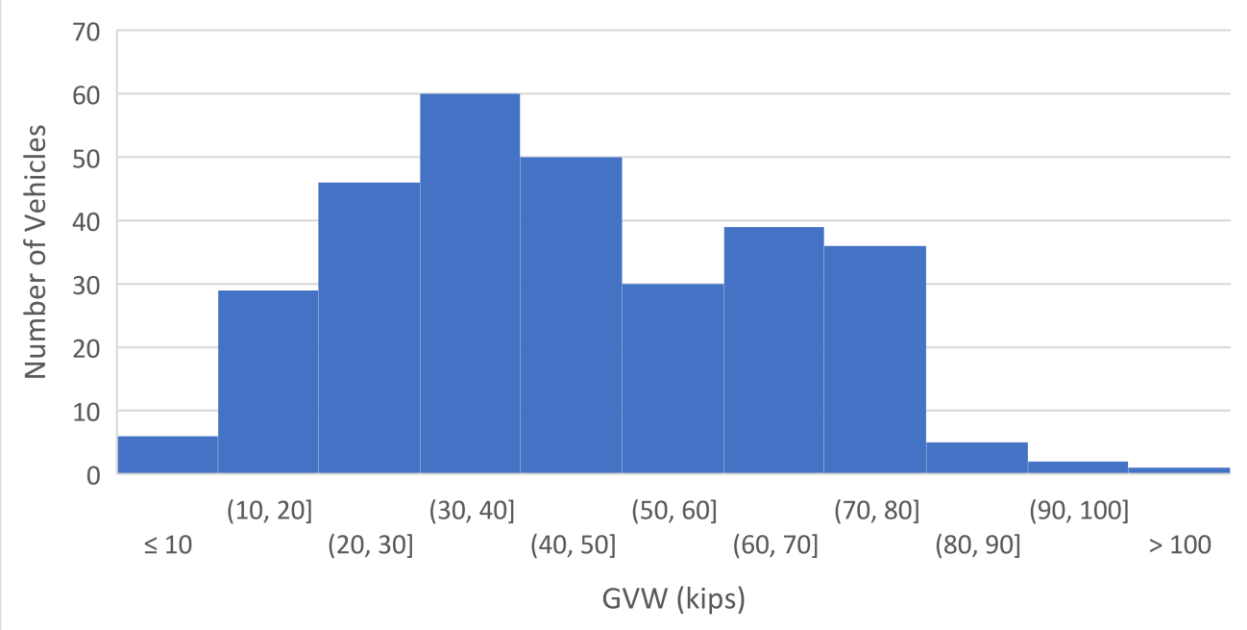

Figure 27: GVW distribution of method 2.

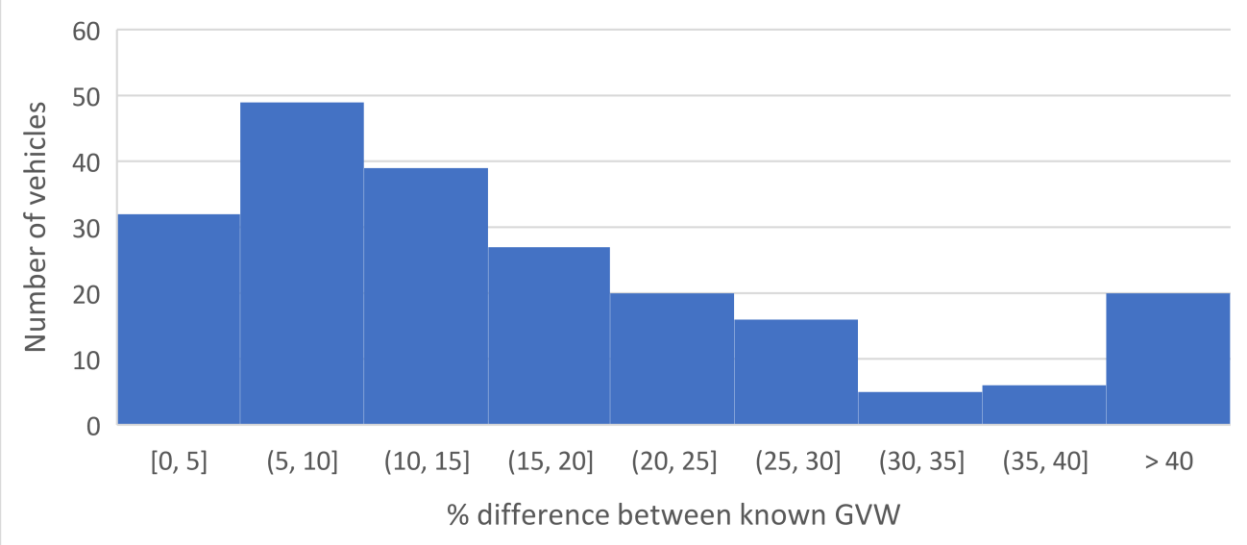

Figure 28: Percent difference between known GVWs of method 2.

As mentioned before a goal for future work is to have these methods work together in one system. This would mean by some machine learning algorithm or photo identification of truck types; the best speed calculation method would be chosen for that particular truck event. With that in mind, if this system was implemented successfully, this would be the result. This shows the best result from the two systems. There are very few vehicles that are over the 15-20% off column. With this distribution, the combined system would receive a grade of D+(20) from the COST323 guidelines. With the increased error of 15%, the grade would be a C(15). The C(15) is a more accurate form of D(20) and is used for the same purposes. With more refining of each method for speed calculation and with the integration of another system to determine truck types, this system could reach higher grades with the intention of bridge and pavement design load determination. The system could also reach the level of enforcements of legal weight limits, which is in the two highest grade categories only 2 grade levels above a C(15).

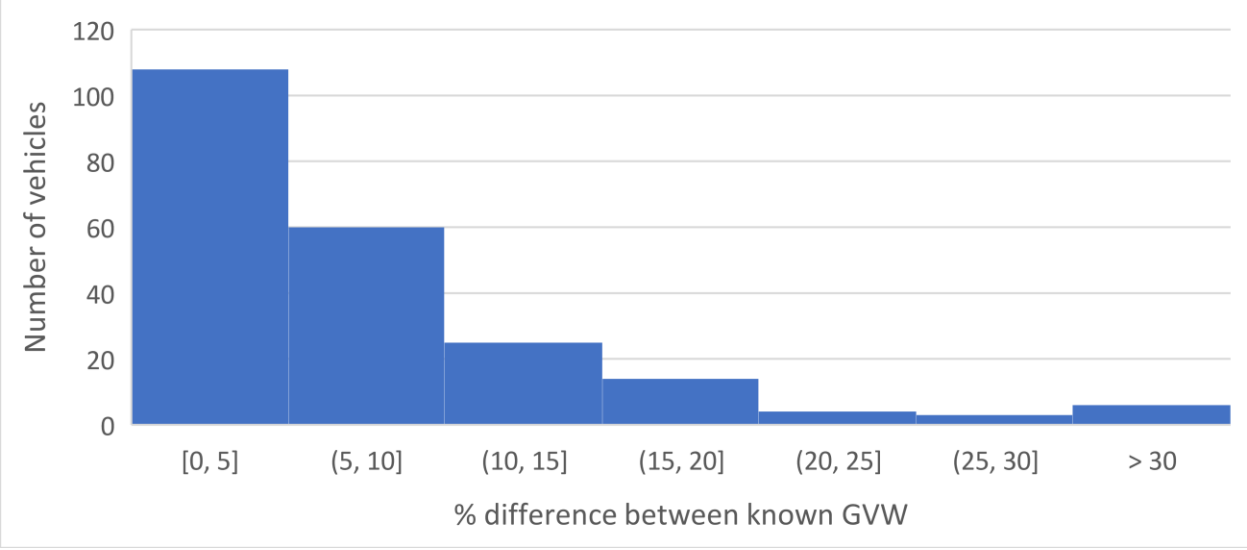

Figure 29: Percent difference between known GVWs of the combined method.

As of this writing, there is no specifications for a BWIM system. Cost 323 refers to all WIM (weigh in motion) system, which is the closest to a BWIM system there is. WIM systems are generally more costly, less safe, but are easier to obtain GVWs from due to the fact that the bridge dynamics are not involved. When specification for a BWIM is released, the grades will have to be adjusted to that new specification.

With the results of the two methods individually and the two methods combined, the algorithm refinement has built greatly on the work of Ojio and Yamada. Adapting their theoretical methodology into a practical one requires much fine tuning and incorporating the two different speed calculating methods can account for more variables that can appear in the field. The improvement in results shows this method can be advanced even further. Extensive tuning of many of the constants listed in the algorithm can be done, but not by human methods. Machine learning is a very viable way to perform this. The machine learning can also help determine which method for speed calculation is the best for which truck type. With the optimized constants and the best speed calculation method chosen, this algorithm can prove to be a valuable step in obtain perfect BWIM.

4.7 Conclusions

This section presented the work on refinement and evaluation of BWIM methods based on the work of Ojio and Yamada. Much effort was focused on the most susceptible to field errors part of their methodology, speed calculation. Two speed calculation methodologies were used from Wall and Lobo-Aguilar respectively, and both methods were refined to work optimally with this data set. This data set was set up and collected from a bridge in Meriden, CT where a BWIM

system was set up in previous research. The results of this research show the speed calculation methods still need some refining, but when used in tandem, greatly improve the results.

CHAPTER 5. CONCLUSIONS

The performance of two systems for the advancement of SHM have been presented in this report. A RFID based crack detection system that works with UHPC, and a BWIM algorithm that uses very few sensors located on the underside of an in-service bridge. The RFID system shows the potential for a field applicable low-cost RFID crack detection system. Using two readers, only the handheld system would be used in field deployment, the backscatter power was able to relay the necessary information for crack detection in the novel material UHPC. Using a simple percent difference from original to un-cracked states damage index, a user is easily able to determine whether a crack has been formed. In the lab setting, a volume-based crack damage extent was used to quantify the damage level. This damage extent also used the crack depth, which may not be obtainable in the field, so field user can conclude the depth has increased when neither the length nor width has changed since last inspection. However, this result can be affected by read distance. A test was done to confirm read distance affecting backscatter power and a read distance of one foot was decided on for all tests and the possible field applicability due to high backscatter power results. This system has also been known to be affected by wireless signals such as cell phones. To confirm crack detection results, an effort must be made to eliminate all these signals near the reader during every reading time. The handheld system was able to detect a crack volume as small as 0.0000194 in^3 and as large as 0.00303 in^3. These findings show this low-cost sensor is ready to be researched for field deployment.

The BWIM system was applied to the Meriden Bridge during previous research. This system collected data during four days while the trucks passing over it were being weighed previously at a weight station. Using this data collected, a new BWIM algorithm was created. Based on Ojio and Yamanda, from the STH, the speed and later, the GVW are obtainable. The

speed being determined by two methods. These methods were able to obtain the vehicle speeds and used them to obtain the GVW estimations. With grades E through C assigned to the system through the COST 323 WIM guidelines, this algorithm shows great promise as a way to incorporate different speed calculations and sensors into one system to achieve the highest grade for a WIM system. The system has many benefits over other systems. Using only 1 strain sensor, 2 if two lanes are being monitored, and 2 accelerometers, 4 for 2 lanes, the system was able to achieve a D (20) rating from COST 323. The system is very safe, placing sensors under the bridge and out of the way of traffic will protect the workers that are needed to install and, not often, maintain the system. Dependence on pavement condition is low, which some systems need to have high good pavement rating to incorporate their methods. If the pavement condition is very low, this system would still be affected, but it is not a factor when the bridge falls under the COST 323 WIM system guidelines. These sensors are also not visible to the public traveling over the bridge. When the system reaches the legal enforcement rating, this is a key benefit because drivers will not alter their normal speeds or travel paths which can affect the data quality. The vision is to improve the algorithm with machine learning or truck photo identification to be able to enforce legal truck weights that are off their designated path in real time to law enforcement. This would help maintain the United States infrastructure by being used only for weights it was designed for.

In summary, both research projects have moved the SHM community forward. Incorporations of novel materials into SHM must be done to keep up with the expanding construction techniques. Fully accurate BWIM systems still allude researchers, but yet another step has been taken to achieve this goal.

CHAPTER 6. FUTURE WORK

While a comprehensive contribution has been made by the research in this study, future studies are suggested to extend the developed framework to be applicable for various full-scale civil structures in a long-term manner.

6.1 Field Deployment RFID Sensors for Crack Detection

The next step for RFID-based crack sensor would be preparing the system for field deployment. All tests were done in the constant environment field of the laboratory and as such, outside tests are needed. With this field deployment comes environmental uncertainties. Many of these uncertainties can create research projects themselves as part of the overall sensor development process. First, a new field ready application process for the tag needs to be developed. It also needs to be easily repeatable for mass deployment. Second, the effect of the weather, such as the sun, humidity, and other conditions need to be carefully considered. Third, the effects of strain from live loads can create tension on the tag and can enlarge the crack. This effect is known to open the crack further, which will have a direct correlation on the mean RSSI. These two coupled have unknown effects on the tag and will need to be studied further to ensure the tags use on not just structure decay cracks, but also loading cracks. All these unknowns would have to be investigated or quantified to prepare the system for full field deployment.

6.2 Algorithm Refinement for Bridge Weigh-in-Motion

The BWIM algorithm has room for improvement. The speed calculation is an estimated approach from the bridge dynamics and sometimes cannot correctly estimate the speed. Other studies use additional systems, such as video or speed strips to calculate the speed. With these

implemented, the GVW calculation would improve. As with many BWIM algorithms, all variables cannot be accounted for. Vehicle lane changes, multiple presence, traffic, speed changes, and very slow-moving vehicles have either been assumed to not occur or the data has not been used. In reality, these occurrences are very real and can be quite often. A multiple system BWIM setup could be the most accurate way to find the GVW. The last restriction of this BWIM research mentioned here is the sample size. With only parts of four days of weight station data to match with the BWIM data, the sample size is not large enough to represent the population. More samples suggest that the sample can be more representable of the population.

REFERENCES

Acheampong, A., Ayarkwa, J., Adom-Asamoah, M., & Baiden, B. (2013). Comparative Study of the Physical Properties of Palm Kernel Shells Concrete and Normal Weight Concrete in Ghana. *J. Sci. Multidiscip. Res.*, 5, 129-146.

Aftab, M., & Karim, H. (2018). A case for structural health monitoring (SHM) and civionics enhances the evaluation of the load carrying capacity of aging bridges. *Innovative Infrastructure Solutions*.

Aktan, E., Culmo, M., Frangopol, D., French, C., & Rabbat, B. (1999). *Committee on Concrete Bridges.* TRB.

Alien. (2019, 1 15). *AtlasRFIDstore.* Retrieved from Alien: http://www.atlasrfidstore.com/alien-short-rfid-white-wet-inlay-aln-9662-higgs-3/

ASCE. (2017). *Report Card for America's Infrastructure.* Reston, VA: American Society of Civil Engineers. Retrieved from Available online: http://www.asce.org (accessed on 15 January 2019).

ASTM Standard. (1994). *E1318-09.* West Conshohocken: ASTM.

Ataur, M., & McQuacker, T. (2016). Application of Ultra High Performance Concrete in Expediting the Replacement and Rehabilitation of Highway Bridges. *First International Interactive Symposium on UHPC.* Ontario: Ministry of Transportation of Ontario.

Azhari, F., & Banthia, N. (2012). Cemenet-based sensors with carbon fibers and carbon nanotubes for piezoresistive sensing. *Cemenet Concrete Composium. 34*, 866-873.

B., G. (2013). *Development of Non-Proprietary Ultra-High Performance Concrete for Use in the Highway Bridge Sector.* Washington DC: U.S. Department of Transportation/Federal Highway Administration.

Caizzone, S., & DiGiampaolo, E. (2015). Wireless Passive RFID Crack Width Sensor for Structural Health Monitoring. *IEEE Sens. J.*, 15, 67-74.

Carden, E. P., & Fanning, P. (2004). Vibration based condition monitoring: a review. *Structural Health Monitoring: 3(4)*, 355-377.

Chang, P., & Alfred, S. (2017). *Building Construction. In Encyclopedia Britannica.* Chicago, IL: Encyclopedia Britannica Inc.

Chen, S.-Z., Wu, G., & Feng, D.-C. (2019). Damage detection of highway bridges based on long-gauge strain response under stochastic traffic flow. *Mechanical Systems and Signal Processing 127*, 551-572.

Christenson, R., Motaref, S., & McDonnell, A. (2012). A Dual Purpose Bridge Monitoring and Weight-in-Motion System for a Steel Girder Bridge. *Proceedings of the International Conference on Weigh-In-Motion (ICWIM 6)*, (pp. 397-408).

COST 323. (2002). *COST 323.* Paris: Laboratoire Central des Ponts et Chaussees.

Division of Systems Information, Bureau of Policy and Planning. (2015). *2015 Traffic Volumes State Maintained Highway Network (Traffic Log).* Newington CT: FHWA.

Doiron, G. (2016). PIER REPAIR/RETROFIT USING UHPC: EXAMPLES OF COMPLETED PROJECTS IN NORTH AMERICA. *First International Interactive Symposium on UHPC.* Des Moines, Iowa.

Donelli, M. (2018). An RFID-Based Sensor for Masonry Crack Monitoring. *Sensors 18*.

Ductal. (2017, September 28). *Ultra-High Performance Concrete (UHPC).* Retrieved from Ductal: http://www.lafargeholcim.us/ductalr-ultra-high-performance-concrete-uhpc

Ekenel, M., Rizzo, A., Myers, J., & Nanni, A. (2005). Effects of Fatigue Loading on Flexural Performance of Reinforced Concrete Beams Strengthened with FRP Fabirc and Pre-Cured Laminate Systems. *Third International Conference on Composites in Construction*, (pp. 405-412). Lyon, France.

FHWA. (2004). Rules and Regulations. *Federal Register Vol. 69 No. 239*, 74419-74439.

FHWA. (2017). *National Bridge Inventory.* Washington, DC: U.S. Department of Transportation.

Gaunt, J., & Sutton, D. (1981). *Highway Bridge Vibration Studies.* Joint Highway Research Project: School of Civil E ngineering, Purdue University.

Goble, G., Moses, F., & Pavia, A. (1976). APPLICATIONS OF A BRIDGE MEASUREMENT SYSTEM. *Transportation research record.*, 579, 36-47.

Google Maps. (2019, 5 12). Map of Meriden Bridge. *Google Maps*. Map.

Graybeal, B. (2011). *Ultra-High Performance Concrete; TechNote.* McLean, VA: FHWA-HRT-11-038; Federal Highway Administration.

Haber, Z., & Graybeal, B. (2016). Performance of Different UHPC-Class Materials in Prefabricated Bridge Deck Connections. *Proceedings of the First International Interactive Symposium on UHPC.* Des Moines, IA: First International Interactive Symposium on UHPC.

Hasgul, U., Turker, K., Birol, T., & Yavas, A. (2018). Flexural behavior of ultra-high-performance fiber reinforced concrete beams with low and high reinforcement ratios. *Struct. Concr.*, 19, 1577-1590.

Huanghuang, H., Xiaojian, G., & Ailian, Z. (2018). Numerical simulation and visualization of motion and orientation of steel fibers in UHPC under controlling flow condition. *Elsevier*, 624-636.

Huynh, T. C., Kim, J. T., & Lee, S. Y. (2016). Structural Identification of cable-stayed bridge under back-to-back typhoons by wireless vibration monitoring. *Measurement 88*, 385-401.

Jin-Hee, A., Shigenobu, K., & In-Tae, K. (2013,). Shear failure behaviors of a web pane lwith local corrosion depending on web boundary conditions. *Elsevier*, 17, 302-317.

Kalansuriya, P., Bhattacharyya, R., & Sarma, S. (2013). RFID tag antenna-based sensing for pervasive surface crack detection. *IEEE Sens. J.*, 13, 1564-1570.

Kalansuriya, P., Bhattacharyya, R., Sarma, S., & Karmarkar, N. (2012). Towards Chipless RFID-Based Sensing for Pervasive Surface Crack Detection. *IEEE 2012 International Conference on RFID -Technologies and Applications (RFID - TA)*, (pp. 6-12).

Kilie, G., & Unluturk, M. S. (2015). Testing of Wind Turbine towers using wireless sensor network and acceleromters. *Renewable Energy 75*, 318-325.

Kim, J., Lynch, J., Zonta, D., Yun, C., Lee, & J.J. (2009). Modal Analysis of the Yeondae Bridge using a Reconfigurable Wireless Monitoring System. *Proceedings of the International Conference on Structural Safety and Reliability (ICOSSAR).* Osaka Japan.

Kolev, V. (2015). Bridge Weigh-in-Motion Long-term Traffic Monitoring in the State of Connecticut. *Master's Thesis. 838*, http://digitalcommons.uconn.edu/gs_theses/838.

Kumar, R., Schultz, A., & Hourdos, J. (2018, Nov. 1). Enriched Sensor Data for Enhanced Bridge Weigh-in-Motion (eBWIM) Applications. Department of Civil, Environmental, & Geo- Engineering.

Leonhardt, F. (1977). Crack Control in Concrete Structures. *IABSE Surveys*, *S-4/77*, 1-26.

Li, J. (2014). *Structural Health Monitoring of an In-Service Highway Bridge with Uncertainties.* Doctoral Dissertation 417., University of Conencticut. Retrieved from http://digitalcommons.uconn.edu/dissertations/417

Liu, J., Wu, C., Su, Y., Li, J., Shao, R., Chen, G., & Liu, Z. (2018). Experimental and Numerical Studies of Ultra-High Performance Concrete Targets Against High-Velocity Projectile Impacts. *Eng. Struct.*, 173, 166-179.

Lobo-Aguilar, S. (2018). Advances in Smart Structure Technologies for Civil Infrastructure. *Doctoral Dissertations. 1870.* . opencommons.uconn.edu.

Martínez-Castro, R. (2018). *Structural Health Monitoring of Critical Load-Carrying Members.* Mansfield, CT: University of Connecticut Graduate School.

Martínez-Castro, R., Jang, S., Nicholas, J., & Bansal, R. (2017). Experimental Assessment of an RFID-Based Crack Sensor for Steel Structures. *Smart. Mater. Struct.*, 26, 085035.

McGovern, B., & Randall, A. (2001). *Connecticut Bridge Inspection Manual.* Newington, CT: Connecticut Department of Transportation.

McGovern, J., & Randall, A. (2001). *Bridge Inspection Manual Version 2.1.* Newington, CT: Connecticut Department of Transportation.

Moses, F. (1979). Weigh-in-Motion System Using Instrumented Bridges. *Transportation engineering journal of ASCE*, 3, 233-249.

O'Brien, E., Znidaric, A., & Dempsey, A. (1999). Comparison of two independently developed bridge weight-in-motion systems. *Heavy Vehical Systems*, 147-161.

Ojio, T., & Yamada, K. (2002). Bridge Weigh-In-Motion System Using Stringer of Plate Girder. *Pre-proceedings of the Third International Conference on Weigh-In-Motion*, (pp. 209-218). Orlando.

Ojio, T., Carey, C. H., Obrien, E., Doherty, C., & Taylor, S. E. (2016). Contactless Bridge Weigh-in-Motion. *ASCE 21*.

Pour-Ghaz, M., Barrett, T., Ley, T., Materer, N., Apblett, A., & Weiss, J. (2014). Wireless Crack Detection in Concrete Elements Using Conductive Surface Sensors and Radio Frequency Identification Technology. *ASCE*, 923-929.

R.E., M.-C. (2018). *Structural Health Monitoring of Critical Load-Carrying Members.* Mansfield, CT: University of Connecticut Graduate School.

Rennane, A., Abdelnour, A., Kaddour, D., Touhami, R., & Tedjini, S. (2018). Design of passive UHF RFID sensor on flexible foil for sports balls pressure monitoring. *IET Microwaves, Antennas & Propagation 12*, 2154-2160.

Russell, H. (2009). *Synthesis of Highway Practice 393: Adjacent Precast Concrete Box Beam Bridges: Connection Details.* Washington D.C.: Transportation Research Board of the National Academies.

Russell, H., & Graybeal, B. (2013). *Ultra-High Performance Concrete: A State-of-the-Art Report for the Bridge Community.* Turner-Fairbank Highway Research Center: Federal Highway Administration, Research and Developement, and Technology.

Saradar, A., Tahmouresi, B., Mohseni, E., & Shadmani, A. (2018). Restrained Shrinkage Cracking of Fiber-Reinforced High-Strength Concrete. *Fibers*, 6, 12.

Sekiya, H., Kubota, K., & Miki, C. (2017). Simplified Portable Bridge Weigh-in-Motion System Using Accelerometers. *ASCE*.

Shim, J. (2005). *Prediction of Early-Age Cracking of UHPC Materials and Structures: A Thremo-Chemo-Mechanics Approach. Master's Thesis.* Cambridge, MA: Massachusetts Institute of Technology.

Song, G., Li, W., Wang, B., & Ho, S. (2017). A review of rock bolt monitoring using smart sensors. *Sensors*, 17,776.

Sony, S., Shea, L., & Ayan, S. (2019). A literature review of next-generation smart sensing technology in structural health monitoring. *Structural Control Health Monitoring 26*, e2321.

Straser, E. G., & Kiremidjian, A. S. (1998). A Modular Wireless damage Monitoring System for Structures. *Blume Earthquake Eng. Ctr. Stamford Univ.*

Sun, K., Li, M. G., & Ye, L. (2010). Damage identification in thick steel beam based on guided ultrasonic waves. *Material Systems and Structures. 21*, 225-232.

Swagato, D., & Purnachandra, S. (2018). A review of some advanced sensors used for health diagnosis of civil engineering structures. *Measurement 129*, 68-90.

Tuequan, B., Zhicheng, C., Shiyin, W., Yang, X., Zhiyi, T., & Hui, L. (2018). The State of the Art of Data Science and Engineering in Structural Health Monitoring. *High Performance Structures: Building Structures and Materials*, 234-242.

U.S. Department of Transportation. (2016). *Chapter 5 Heavy Vehicals and Charactoristics.* Oak Ridge National Laboratory.

U.S. Department of Transportation, F. (2016). Highway Statistics 2016 Table 3.8. *Transportation Energy Data Book*. Washington DC, Table VM-1 and annual. (Additional resources: www.fhwa.dot.gov): Oak Ridge National Laboratory .

Wall, C., Christenson, R., McDonnell, A.-M., & Jamalipour, A. (2009). *A Non-Intrusive Bridge Weigh-in-Motion System for a Single Span Steel Girder Bridge Using Only Strain Measurements.* Newington: Connecticut Department of Transportation.

Wan-Wendner, L., Wan-Wendner, R., & Cusatis, G. (2018). Age-dependent size effect and fracture characteristics of ultra-high performance concrete. *Cem. Concr. Compos.*, 85, 67-82.

WAVE. (2001). *Weighing-In-Motion of Axles and Vehicals for Europe.* European Commission .

Yuan, J., & Graybeal, B. (2014). Bond Behavior of Reinforcing Steel in Ultra-High Performance Concrete. *FHWA*, Available online: http://www.fhwa.dot.gov/publications/research/infrastructure/.

Yuequan, B., Zhicheng, C., Shiyin, W., Yang, X., Zhiyi, T., & Hui, L. (2018). The State of the Art of Data Science and Engineering in Structural Health Monitoring. *Elsevier, The State of the Art of Data Science and Engineering in Structural Health Monitoring*, Vol 5 Issue 2, 234-242.

Zhang, J., Gui Yun, T., Marindra, A., Imam Sunny, A., & Zhao, A. (2017). A Review of Passive RFID Tag Antenna-Based. *Sensors*, 265.

Zhang, J., Tian, G., Marindra, A. M., Sunny, A. I., & Zhao, A. B. (2017). A Review of Passive RFID Tag Antenna-Based Sensors and Systems for Structural Health Monitoring Applications. *Sensors 17*.

Zhang, Y., & Bai, L. (2015). Rapid structural condition assessment using radio frequency identification (RFID) based wireless strain sensor. *Autom. Constr.*, 54, 1-11.

Zhao, H., Uddin, N., Shao, X., Zhu, P., & Tan, C. (2014). Field-calibrated influence lines for improved axle weight identification with a bridge weigh-in motion system. *Structure and Infrastructure Engineering*, 721-743.